VISUAL SIMULATION IMAGE GENERATION USING A FLYING-SPOT SCANNER

by Charles A. Wagner

Flight Research Center
Edwards, Calif.

NATIONAL AERONAUTICS AND SPACE ADMINISTRATION • WASHINGTON, D. C. • APRIL 1969

VISUAL SIMULATION IMAGE GENERATION USING A FLYING-SPOT SCANNER

By Charles A. Wagner

Flight Research Center
Edwards, Calif.

NATIONAL AERONAUTICS AND SPACE ADMINISTRATION

For sale by the Clearinghouse for Federal Scientific and Technical Information
Springfield, Virginia 22151 – CFSTI price $3.00

CONTENTS

VISUAL SIMULATION IMAGE GENERATION USING A FLYING-SPOT SCANNER

By Charles A. Wagner
Flight Research Center

SUMMARY

This paper analyzes the flying-spot scanner television camera used as a video signal generator for visual flight simulation. A description of the technique is included as well as a detailed theoretical analysis of the quality of the video that can be produced. A commercially available flying-spot scanner designed for flight simulation was tested, and its capabilities are presented. Discussion is limited to the television camera; display devices such as monitors are not included.

The flying-spot scanner was found to be a low-cost device which can simulate all motions of an aircraft except roll. Large excursions at high rates are easily achieved. It is limited to a relatively small field of view, a fixed forward visibility, and simulation of flat terrain. The quality of the video is adequate over a moderate range of altitudes; very high and very low altitudes result in poor performance. Possible approaches to increasing the useful altitude range are discussed.

INTRODUCTION

In flight simulation, a display is required that represents the outside world as seen from the cockpit of a flying aircraft. Generating this display (visual simulation) is difficult because a large dynamic range is encountered and a great deal of information must be presented. Many devices have been constructed that attempt to achieve this goal. Examples include film-based display devices, computed displays, direct optical viewing devices, and television-based devices. Each class of device has its characteristic advantages and limitations. The selection of the best visual simulation device for a given application requires a knowledge of the capabilities and limitations of those available. Some visual simulators have been thoroughly analyzed in the literature, but little information is available on the flying-spot scanner television camera used as a video signal generator for visual simulation.

This paper describes and analyzes the flying-spot scanner adapted to visual simulation. Since the flying-spot scanner is a television camera, its performance is evaluated by the quality of the video signal it produces. Television display devices are adequately described in the literature; therefore, only those features of the final picture that are inherent in the flying-spot scanner video signal are discussed in this paper.

This paper contains a general description of the flying-spot scanner technique. Also included is a detailed theoretical analysis of the video signal that can be produced utilizing this technique. A commercially available flying-spot scanner designed for visual simulation was available for experimental purposes. This unit was tested extensively, and the results of the tests are presented. The performance of the tested flying-spot scanner is compared to that predicted by the theoretical analysis. Although the tested unit may not necessarily reflect the limit of the state of the art in flying-spot scanner technology, it serves as an example of what has been achieved using actual hardware. Subjective comments on the picture produced by the tested unit are also included, inasmuch as they may convey information not apparent from the analytical results.

SYMBOLS

A	area
B	luminance or brightness
$B(\lambda)$	relative spectral-power distribution of a radiating blackbody at 2870° K as a function of wavelength of light
C	nondimensional spatial frequency, $\frac{n\pi S}{L}$
D	length of phosphor decay tail from maximum to $1/e_n$ of maximum
d	duty cycle of raster (fraction of time raster is on)
$E(\lambda)$	relative sensitivity of standard human eye as a function of wavelength of light
e	electronic charge (approximately 1.6×10^{-19} coulombs)
e_n	base for natural logarithms (2.718 . . .)
F	luminous flux
Δf	bandwidth
G	normalized transfer admittance based on scanning spot exclusive of decay tail, $\frac{Y(n)}{2S}$
G′	normalized transfer admittance based on scanning spot including decay tail, $G/\lvert G\rvert_{c=0}$

g	transmission efficiency of optical system
h	scaled altitude of aircraft
I	luminous intensity
$i = \sqrt{-1}$	
i_k	photocathode current
K	spectral correction factor
L	half the length of a scan line
l	horizontal viewing angle, positive to right
M	magnification of optical system
N	relative aperture (f-number) of optical system
n	number of complete cycles in a scan line
$P(\lambda)$	relative spectral-power distribution of a glowing phosphor as a function of wavelength of light
Q	nondimensional transition point, $\frac{Z_1}{S}$
R	ratio of decay tail length to spot size, $\frac{D}{S}$
S	size of scanning spot exclusive of decay tail between half-amplitude points
S'	measured width of spot when scanned past a slit
S_k	photocathode sensitivity
S/N	ratio of signal to noise
$S(\lambda)$	relative sensitivity of a photocathode as a function of wavelength of light
T	relative signal distribution in scanning spot
t	time
V	scan velocity measured on cathode-ray tube
v	vertical viewing angle, positive upward

W	width of slit used in slit-scanning
x	vertical coordinate on flying-spot scanner raster
Y(n)	equivalent transfer admittance
y	horizontal coordinate on flying-spot scanner raster
Z	dimension in direction of scan
Z_1	transition point between cosine and exponential portions of scanning spot
θ	pitch angle of aircraft, positive upward
λ	wavelength of light
ψ	solid angle subtended by optical system

Subscripts:

c	cosine portion of spot profile
d	relating to phosphor decay characteristic
e	exponential portion of spot profile
max	maximum value of parameter
p	relating to signal-processing circuit characteristic
r	relating to cathode-ray tube raster
s	relating to cathode-ray tube spot
u	relating to phosphor rise characteristic

DESCRIPTION OF THE FLYING-SPOT SCANNER

Principles of Operation

Flying-spot scanners have been used in commercial television for generation of video from slides and have been adapted for televising motion pictures. These uses have largely given way to other techniques. However, the flying-spot scanner (FSS) is by no means obsolete. It has the capability of extracting data from finely detailed slides.

The principle of operation of the FSS is shown in figure 1. A special-purpose cathode-ray tube (CRT) with a fast-decay phosphor generates a moving point source of light. The relay lens focuses the point source onto a slide transparency. The

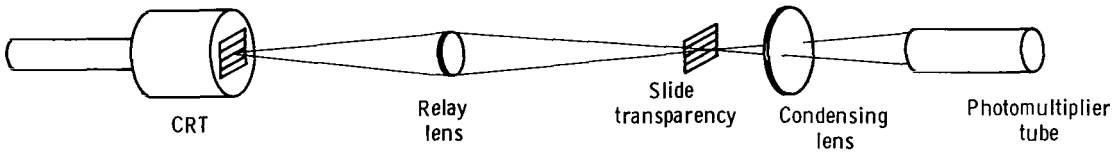

Figure 1.– A typical flying-spot scanner.

fraction of light transmitted through the slide is proportional to the transmission of the slide at that point. The condensing lens directs the light onto the photocathode of a photomultiplier tube. Thus, the output of this tube is proportional to the transmission of the slide at the point in question. If the moving point source is tracing out a rectangular raster (scanning pattern), the output of the photomultiplier tube (suitably amplified) becomes a video signal whereby the image on the slide can be reproduced on a television monitor.

Assuming the slide is a plan view of an airport and surrounding terrain, the reconstructed image will appear as though it were viewed vertically downward from an airplane. Such a view is generally of no particular use in visual flight simulation. A perspective view is required which represents the terrain as seen from any arbitrary altitude at any arbitrary angle. A technique for producing a perspective view is described in reference 1.

When the FSS raster size decreases (the monitor raster size remaining constant), less area from the slide is reproduced on the monitor. Therefore, the viewed area appears magnified. This assumes that, although the FSS raster is smaller, each scan line still requires the same length of time and the same number of scan lines is used. A perspective view of an object (particularly, flat terrain) can be constructed by magnifying that portion nearest the observer to a greater extent than that which is farther away. This is done by scanning areas of the slide near the observer with short scan lines closely spaced, and scanning areas of the slide farther from the observer with longer scan lines more widely spaced. The display raster on the television monitor retains its normal size and shape at all times. The position of the scanning spot on the FSS raster is a function of the position of the scanning spot on the display raster as well as the altitude and pitch angle of the simulated aircraft. Equations for computing the FSS raster are derived in appendix A. Figure 2 shows a typical FSS raster envelope with a few scan lines. As shown in appendix A, the boundaries of the raster are straight lines; thus it is always trapezoidal. Altitude and pitch changes are simulated

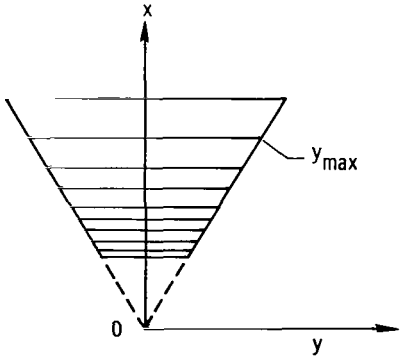

Figure 2.– A typical flying-spot scanner raster envelope.

merely by electronically computing the appropriate FSS raster for each condition; physical motions of components are not required.

Figure 3 is a pictorial representation of this special-purpose FSS. The observer at $0'$ is looking through a window at the transparency. It is desired to replace the window with a television screen. Every point on the window (that is, the television screen) can be projected to some corresponding point on the transparency by extending a straight line from the observer through that point on the window to the transparency plane. It is only necessary to "paint" the same point-by-point brightness on the television screen as the observer would see when looking through the window. The FSS determines the brightness of each point on the television screen by placing its scanning spot at the corresponding point on the transparency, measuring the transmission, and sending the appropriate signal back to the television set.

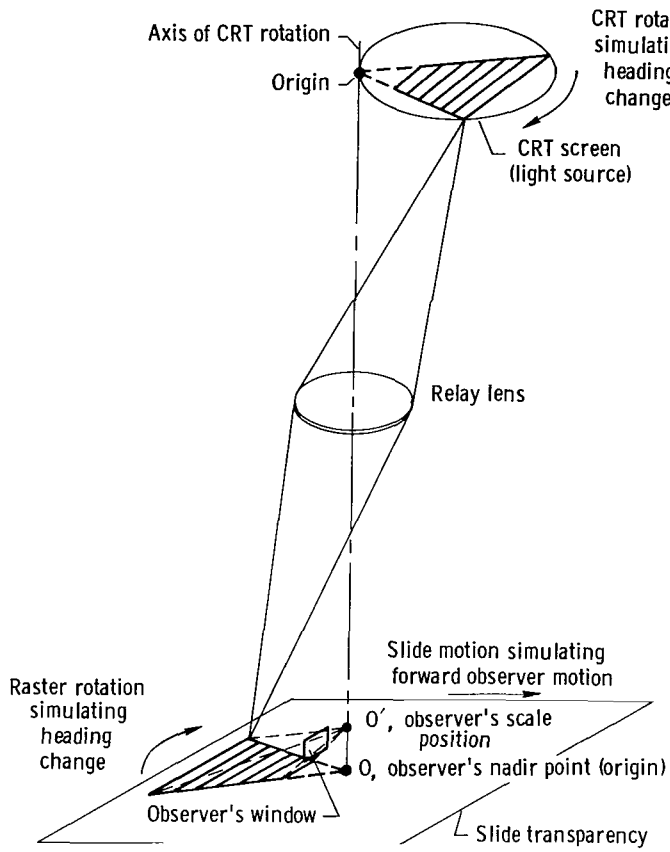

Figure 3.– A flying-spot scanner television camera forming a perspective view of a plane transparency.

Also shown in figure 3 are the techniques for simulating heading changes and forward motion. Rotation of the CRT about the axis shown effectively pivots the observer and his window to some different heading angle. Moving the slide in its own plane gives the observer the impression that he is moving longitudinally or laterally. The FSS does not simulate the effect of aircraft roll; the display device (that is, the monitor) must simulate the aircraft roll angle.

Two scale factors are found in the FSS. One is the scale factor of the transparency, where scale factor is defined as the ratio of a dimension on the transparency to the corresponding dimension in the real world. The same scale factor also applies to the image of the scanning raster, which is on the transparency. The scanning raster itself, on the CRT screen, will not be the same size if the relay lens does not operate at a magnification of unity. Therefore, a different scale factor exists at the CRT raster, which is the transparency scale factor divided by the magnification.

Design Considerations and Limitations

Ideally, a perspective view of terrain should include information all the way to the horizon, which is theoretically an infinite distance away. The FSS inherently cannot produce this information because it cannot "see" any terrain beyond the confines of the image of the raster. The limited size of the raster image places a fixed upper limit

on forward visibility. At low altitudes the fixed forward visibility is practically unnoticeable because a bit of detail which is scanned by the raster line farthest from the origin lies very near the horizon. However, at high altitudes this same bit of detail will appear well below the correct horizon position. There are several ways to handle the problem. One is to display a simulated sky (generated by a sky computer) covering all portions of the picture where no terrain exists. The result is a horizon position that is too low. Another approach is to fill in this gap with a computed presentation different from the sky, which may represent haze or some other limit to visibility. This presentation correctly locates the horizon. Figure 3 shows a design that makes maximum use of the available area on the CRT. The origin is at one edge of the screen, and the raster is as large as possible. This arrangement maximizes forward visibility.

The previous discussion has assumed that the CRT produces a point source of light. In reality, this "point" source has appreciable dimensions. The consequences of spot size are analyzed in detail in the following sections of this paper. However, a general idea of spot-size effects is necessary for an understanding of design trade-offs. One rule of thumb states that the smallest bit of detail that can be detected is roughly the same size as the scanning spot.

The proper choice of a raster scale factor is far more important than the choice of a transparency scale factor. Maximizing forward visibility requires choosing a small raster scale factor, where a large distance in the real world represents a very small distance on the CRT. However, the CRT spot size will then limit the smallest detectable detail to objects that are large in the real world. Thus, at low altitudes the small details that the observer expects to see close to his window will be lost, and his picture will be poor. Therefore, detail size is traded against forward visibility. The best CRT is the one that provides the smallest spot size near the origin compared to the total screen size. This is not quite the same requirement that is important for most scanner tubes; namely, that they produce a large number of distinct spot diameters across the screen. This particular CRT needs small spots only in one area on the screen. Magnification cannot improve this situation because it magnifies the spot along with the raster and does not improve the ratio of spot size to screen size. A given raster can be optically magnified or demagnified to match various transparency scale factors with essentially no change in the final picture. Thus, the transparency scale factor becomes a secondary consideration, governed mainly by optical parameters.

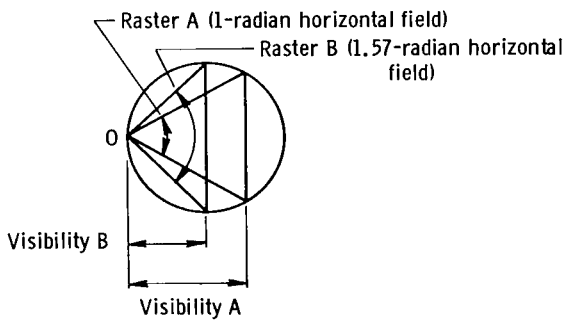

Figure 4.– Relationship between field of view and forward visibility.

The horizontal field of view is the angle between the sides of the raster when the simulated aircraft is in level flight. Figure 4 shows a scanner-tube screen with two raster envelopes. Raster A corresponds to a 1-radian horizontal field, and raster B corresponds to a 1.57-radian horizontal field. With no change in magnification, there is a significant loss in forward visibility with the larger field. By making up the loss in visibility with increased magnification, there is a loss in detectable detail, since the spot size becomes larger. Forward visibility could be increased with a

reduction in horizontal field of view. However, the maximum possible increase is small (33 percent) and would require a severe reduction in the horizontal field. The 1-radian field appears to be an excellent choice because it utilizes the greatest possible fraction of the round screen of the scanner tube.

Vertical field of view is governed largely by the fact that roll is produced by the display device. In order to fill the pilot's window at all roll angles, the vertical and horizontal fields of view should be equal.

Effects of Three-Dimensional Terrain

As designed, the FSS inherently cannot produce the effects of three-dimensional terrain. The terrain always appears perfectly flat, since all detail within the pilot's field of view is always visible (even though in the real world some detail is hidden behind buildings, mountains, etc.). If the terrain is represented by a plane transparency, the third dimension cannot be reproduced, since it is not stored in the transparency. The use of a three-dimensional transparency would not improve the situation. Light strikes the transparency essentially normal to the surface, and the quantity of transmitted light determines the brightness of that point. Therefore, even though the light strikes the top of a simulated mountain, there is nothing to indicate elevation, since the signal is identical to that which would be received from a plane transparency having the same density variation.

The missing third dimension is not particularly noticeable at higher altitudes, but it becomes quite apparent near the ground, particularly if buildings are near the position of the aircraft. Roofs of hangars look like rectangular pads painted on the ground. It is evident that the FSS cannot be used as an aircraft simulator where three-dimensional effects must be included, such as for visual terrain-avoidance studies.

At least one type of FSS has been constructed that includes the third dimension. The principle of operation requires two transparencies to be scanned simultaneously, one containing terrain brightness and the other containing elevation information. The scan format is radial from the aircraft position outward. A high-speed computer operates from the elevation information and controls the display scan to provide occultation and appropriate magnification changes to sloped terrain.

Further consideration of this principle is beyond the scope of this investigation. It is mentioned to indicate another design possibility for the FSS. Further information on this principle is presented by Caligiuri in reference 2.

Inherent Capabilities

The FSS is inherently a relatively simple, low-cost device that occupies little space and generates very little heat. It is easy to maintain and operate, does not require frequent adjustments, and uses little power. All components have expected lifetimes greater than a thousand hours. It is highly feasible to maintain a selection of transparencies covering various areas at various scale factors, and these transparencies can be interchanged as rapidly as required.

Unlike a transport designed to carry a television camera over a model, the FSS does not require a complex servosystem which must simultaneously move in three dimensions and rotate about three axes. One simple servo is required to rotate the CRT, and it can be made as powerful as required for any desired rate of heading change. Furthermore, the servo can be designed for continuous heading changes if desired. Since the transparency is not large or heavy, relatively simple servos can move it easily at very high scale speeds. Pitch and altitude changes occur as fast as the raster computer can react. If the origin is located at the edge of the CRT, the maximum negative pitch angle occurs when the scan line at the bottom of the picture crosses the origin. A more negative pitch angle requires terrain behind the origin to be visible. If desired, the origin could be located at some other point on the CRT. The limiting case would be the location of the origin at the CRT center, where unlimited pitch changes could be made.

Characteristics of the Tested Flying-Spot Scanner

A commerically available FSS of the type considered in this paper was tested and evaluated. The entire unit, including electronics, requires a floor space about 2 meters by 2 meters. It produces a 1-radian horizontal field of view, a 0.7-radian vertical field of view, and has a haze generator which properly locates the horizon. The television system operates at the standard 525-line, 30-frame-per-second rate.

The scale factor measured at the CRT raster is 1/54,000. The CRT screen has a diameter of 108 millimeters. The origin of the raster is at the edge of the screen. Inscribing the raster triangle in this circle shows that the maximum forward visibility is 81 millimeters, which is a scale 4.4 kilometers.

The square transparency is 0.5 meter on a side, has a scale factor of 1/60,000, and contains a square terrain segment 30 kilometers on a side. The transparency servos are capable of simulating horizontal speeds up to 300 meters per second.

The servo which rotates the CRT is capable of simulating continuous heading changes of unlimited magnitude, since electrical connections to the CRT are made through slip rings. The maximum rate of heading change is 1 radian per second.

The maximum downward pitch angle is limited to 1.2 radians, because a larger angle requires terrain behind the origin to be visible. Upward pitch angles greater than 0.35 radian produce a display that is all sky. A pitch change from one extreme to the other can occur in one television frame time (1/30 sec).

An altitude of 800 meters coupled with the 4.4-kilometer forward visibility yields a level-flight picture with terrain in the lower fourth, haze in the next fourth, and sky in the upper half. This appears to be a maximum practical altitude. A minimum altitude of 3.6 meters can be simulated, but no fine detail can be seen near the observer's position. The maximum vertical speed is limited by the raster computer to 150 meters/second.

METHODS OF VIDEO ANALYSIS

The quality of the video signal produced by the FSS and the capabilities of the display device determine the quality of the final picture. Display devices were not part of this investigation; only the quality of the video signal was considered. In this section, the video signal is analyzed in objective terms.

Video is judged primarily by signal-to-noise ratio, frequency content, and gamma. If signal-to-noise ratio is too low, the picture will have "snow" in it. Video that does not have high-frequency components will produce a smeared picture lacking fine detail. Gamma is a measure of the overall linearity of the camera and the display device together. Here, linearity refers to the brightness variations in the final picture as compared to the brightness variations of the object being photographed. The FSS is inherently a linear device. Therefore, gamma will not be considered further.

Signal-to-Noise Ratio

The primary source of random noise in the FSS is shot noise from photocathode emission. Photomultiplier tubes can produce large outputs, and good amplifiers are available which can process this signal without adding appreciably to the noise.

Computation of the signal-to-noise ratio requires knowledge of the quantity of light reaching the photocathode. Most light-quantity measurements are made with sensors which have essentially the same spectral response as the human eye. A simple way to measure light output from a CRT is to measure the brightness of a uniform raster with an eye-corrected photometer. Photocathode sensitivity is frequently given in terms of light from a tungsten filament lamp operated at a color temperature of 2870° K, which closely matches visible blackbody radiation at that temperature. A CRT source and a blackbody source could be adjusted to produce the same amount of light as far as the eye is concerned. However, the photocathode might find them quite different from each other because the sources do not produce the same emission spectrum and the spectral response of the photocathode is not the same as that of the eye. There is a need for a way to relate the amount of light emitted from a CRT in terms of eye response to the amount of light that represents excitation to the photocathode. Appendix B presents the derivation of a spectral correction factor K. The light output from a CRT is multiplied by this factor, which essentially converts it to an equivalent amount of light from a blackbody at 2870° K for a particular photocathode. Each factor applies to only one phosphor-photocathode combination. Table I is a list of phosphors and their associated spectral correction factors for a photocathode with S-20 response. The calculations are shown in appendix B.

TABLE I. – SPECTRAL CORRECTION FACTORS FOR AN S-20 PHOTOCATHODE

Phosphor	Spectral correction factor
A-2	0.41
P-16	45
P-24	.87
P-36	.53
P-37	2.5

The remainder of the calculation of signal-to-noise ratio is relatively straightforward and is carried out in appendix C. The final equation is

$$S/N = \frac{0.9}{2N\left(1 + \frac{1}{M}\right)} \left(\frac{\pi S_k g B_r A_r K}{2ed\Delta f}\right)^{\frac{1}{2}} \qquad (1)$$

Another form of noise is also present in the FSS, but it is not random. This noise occurs because the CRT screen is not perfectly uniform, and the light output varies slightly from point to point. The magnitude of this phosphor noise depends on the quality of the screen and is not analytically predictable. Phosphor noise must be measured on the particular CRT used.

Frequency Content

The information content of the video signal is determined primarily by three elements in the scanning system. First, the transparency itself determines the maximum available information. Second, the size of the scanning spot on the CRT limits readout capability. Finally, the relay lens may effectively defocus the spot. The spatial frequency-response technique is used to analyze the information content of the video. This technique makes it relatively easy to analyze independently the capabilities of each of the three elements and to combine them into a single spatial transfer function. Furthermore, spatial frequency response is easily converted to the more familiar time-based frequency response by simply multiplying spatial frequencies by scan velocity.

The determination of the spatial frequency response of a lens is an experimental task and, as such, is dealt with in the next section of this paper. Since the FSS is being analyzed as a camera, the transparency is the input signal. Therefore, its spatial frequency content does not affect the capabilities of the camera. The quality of the transparency should be such that it is not a significant limiting factor in the information content of the video.

It remains to determine the spatial frequency response due to the CRT spot size. This analysis is limited to a one-dimensional scan. Figure 5 shows the spot profile

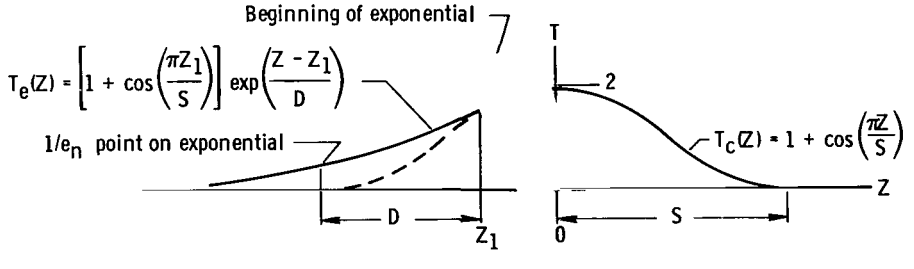

Figure 5.– Profile of cosine scanning spot with decay.

assumed for this calculation. Spot size is defined as the width between the half-amplitude points of the spot profile. The assumed spot has a basic profile with a 1 + cos Z description, and it has an exponential tail. Although a Gaussian profile is usually assumed for the basic shape, both representations are only approximations. Reference 3 shows that there is relatively little difference between transfer functions of various spot profiles in the regions of interest. The exponential tail is intended to approximate the effects of phosphor decay, since all known useful phosphors have decay characteristics that are significant at television scan speeds and are more or less exponential.

The spatial frequency response is computed by taking the Fourier transformation of the spot profile. The computation is presented in appendix D, and figure 6 is a graph of the resulting transfer function. Although the complete expression for the

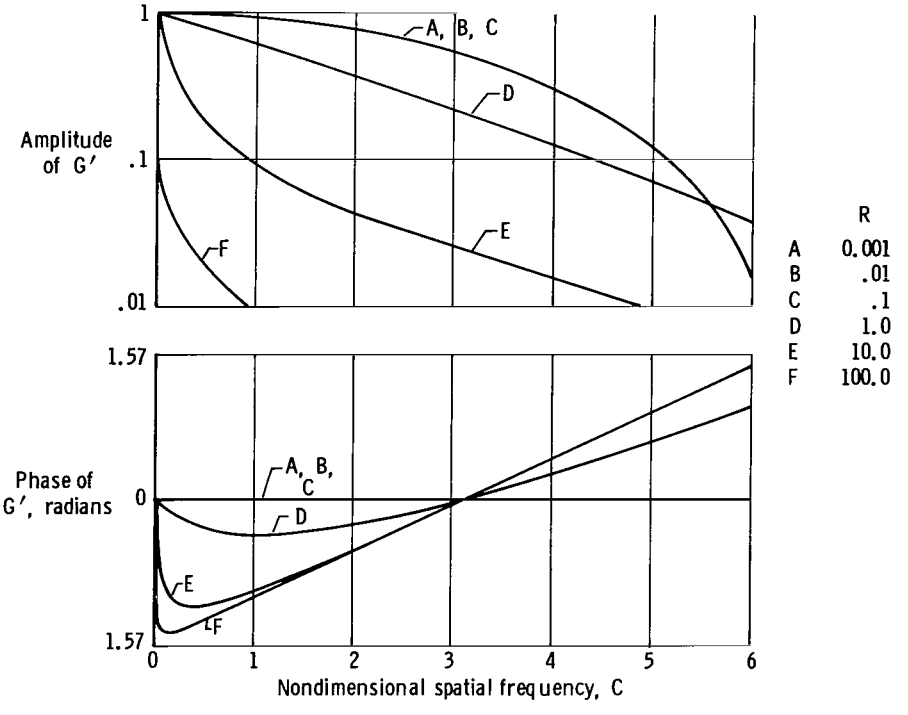

Figure 6.– Normalized transfer admittance versus nondimensional spatial frequency for several ratios of decay length to spot size.

transfer function is somewhat complex (equations (D1) to (D3) in appendix D), it reduces to simple limits for extreme values of R. The case where R is zero corresponds to a situation where the scan velocity is slow enough and the phosphor decay is fast enough to eliminate the effects of the decay tail. The transfer function is

$$G'\Big|_{R=0} = \frac{\pi^2 \sin C}{C(\pi^2 - C^2)} \qquad (2)$$

This result is exactly the same as that obtained in reference 3 with C called rz and G′ called Y(z). Curves A, B, and C in figure 6 correspond to equation (2). The other

limit occurs when R is very large. A large value of R corresponds to a situation where scan velocity is fast enough and phosphor decay is slow enough to form a very long decay tail. In the limit, the actual spot size itself is negligible compared to the decay tail and, for small values of C, the transfer function becomes

$$\lim_{(R \longrightarrow \infty)} G' = \frac{1}{1 + iRC} \tag{3}$$

Curves E and F in figure 6 correspond to equation (3). This transfer function is essentially that of a simple resistance-capacitance filter.

The curves of figure 6 show that when phosphor decay effects can be neglected, there is a definite limit on the detail (spatial frequency) that can be detected by the FSS because of spot size alone. As scan velocity is increased (or a slower decaying phosphor is used), the lengthening decay tail increases spot size, reducing the capability of the FSS to detect small detail at high spatial frequencies. In an FSS where a wide range of scan velocities is encountered, it is not sufficient to make a single simplifying approximation to spot size, since it changes with changing scan velocity. Rather, it becomes necessary to include the composite effect of basic spot size and decay tail length.

The transfer-function method described is limited to linear systems. If a nonlinear device such as a signal-processing amplifier is incorporated in the output circuit, it becomes more difficult to describe the signal analytically. One possible solution to this problem is to program the entire system on an analog computer and compare the output signal directly to the input signal. There are other possible advantages to using an analog computer in addition to handling nonlinear elements. A simplified program and some elementary results are presented in appendix E.

ANALYSIS OF INDIVIDUAL COMPONENTS OF THE TESTED FLYING-SPOT SCANNER

Color Considerations

The tested FSS was originally designed to produce color video. A color scanner can be constructed by using a CRT phosphor which produces a wide visible spectrum (ideally it should produce white light). A color transparency is used in the FSS. The light transmitted through the transparency at each point is the same color as the point on the transparency. A system of dichroic mirrors (fig. 7) splits this transmitted light into three beams—the primary colors, red, green, and blue. Three photomultiplier tubes are used, and each receives the light from one beam. Thus, three simultaneous video signals are provided, one for each primary color.

A number of problems forced the conversion to a monochrome system. One of the more serious problems was a low signal-to-noise ratio in the red channel. The CRT used in this FSS has a P-24 phosphor, which is the best available for color scanners. The photocathode of the photomultiplier tube has an S-20 spectral response, which is

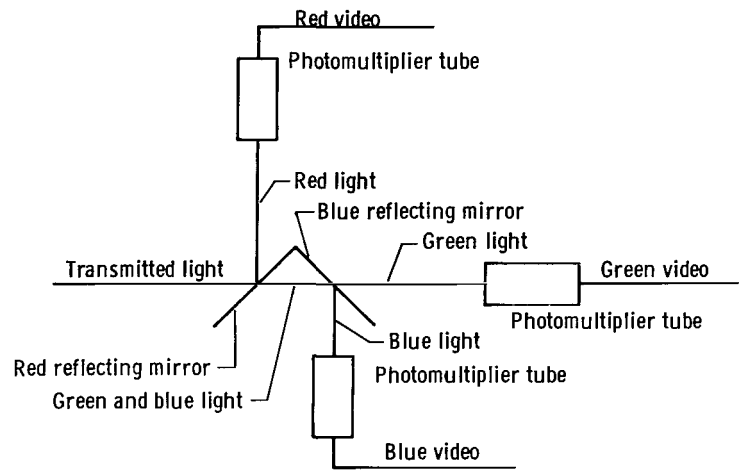

Figure 7.– Color-scanner dichroic-mirror assembly.

also the best available for color scanners. Because this phosphor produces relatively little red light, and because this photocathode is relatively insensitive to red light, the cathode current was low. Thus, the photomultiplier shot noise produced an unacceptable amount of red noise in the picture. Another serious problem was the inability of the system to produce the proper balance of colors. Color balance is a complex problem which arises from illuminating a transparency with light that does not have the same spectral content as "white" light. Furthermore, the transparency does not have the same spectral transmission characteristics as the reflectance characteristics of the real world. Still other problems involved the display device, but they are beyond the scope of this discussion.

The conversion of the FSS to monochrome was easily accomplished by removing the dichroic mirrors from the optical system. Two video channels were thus disabled. The remaining active video channel (which received all the light from the transparency) became the black and white channel. All tests and measurements were made on the system after the monochrome conversion.

Cathode-Ray Tube

The CRT used in this FSS is electrostatically focused, magnetically deflected, and has a flat faceplate with a useful screen diameter of 108 millimeters. A raster triangle inscribed in this size circle shows that the maximum distance of any point on the raster from the origin will be about 94 millimeters, and the longest scan line will also be 94 millimeters. Referring to equation (A10) in appendix A, if the pitch angle θ of the simulated aircraft is zero (level flight) and if the horizontal and vertical fields of view are 1 and 0.7 radian, respectively, the length of the shortest scan line becomes three times the scale altitude. Since the raster scale factor is 1/54,000, an actual altitude of 3.6 meters (representative of an airplane on the ground) produces a scan line only 0.2 millimeter long.

Because of the rather unusual raster that is formed on the CRT, the phosphor is scanned very heavily in the vicinity of the origin (which is at one edge of the tube) and scanned very lightly elsewhere. It is easy to burn the phosphor at the origin if the tube is driven too hard. Thus, from a practical standpoint, phosphor burn controls the light output. Experience has established a set of operating voltages for this CRT which result in satisfactory phosphor life under normal conditions. When these operating voltages are applied and a 5.1-centimeter- by 5.1-centimeter raster with a 0.68 duty cycle is generated, the resulting screen brightness is 63 candelas/meter^2, as measured with an eye-corrected photometer. This brightness is roughly equivalent to a source intensity of 0.24 candela.

Tests on the P-24 phosphor have shown that light output varies with scan velocity. These variations involve both phosphor rise time and decay time. From the derivation in appendix F, it can be inferred that the ratio between exponential rise time and exponential decay time equals the ratio between light output at high scan velocities and light output at low scan velocities. Experiments on the P-24 phosphor showed that this ratio is about 2 to 1. These experiments were conducted by placing the CRT in a light-tight enclosure and exposing it to a photomultiplier tube. The scan velocity was reduced until the light output would reduce no further. Then the scan velocity was increased until the light output would no longer increase. Comparing the signals from the photomultiplier tube yielded the 2 to 1 ratio. Thus, the source intensity of the CRT varied from about 0.13 candela to about 0.26 candela over the range of scan velocities. This conclusion is inferred from the fact that the longest scan lines produced about 10 percent more signal on the photomultiplier than the 5.1-centimeter scan lines of the raster mentioned previously. Generally speaking, raster lines less than 1 millimeter long produce roughly the minimum light, whereas lines greater than 70 millimeters long produce the maximum light. These raster lines are scanned in 45 microseconds.

Spot size was measured by the slit-scan technique. In order to obtain a good signal and minimize errors due to the slit aperture, the setup shown in figure 8 was used. A single-line raster with a slow scan velocity of 7500 millimeters/second was placed on the CRT face. The high quality camera lens has a 50-millimeter focal length and a 35-millimeter field. It was operated in reverse, magnifying the raster by a factor of five. The slit size was measured with a microscope having a calibrated reticle and was found to be less than 0.025 millimeter wide. The output of the photomultiplier was observed on an oscilloscope, and the pulse width at the half-amplitude points was read. Since the ratio of pulse width (in time units) to total time for one scan line equals the ratio of spot size to line length, the spot size on the CRT screen was calculated to be about 0.1 millimeter. From appendix G it is seen that the slit width of 0.025 millimeter compared to the spot size of 0.5 millimeter at the slit resulted in

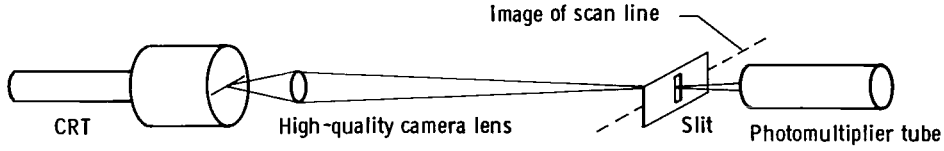

Figure 8.– Slit-scan test setup.

negligible aperture error. The lens is capable of imaging the spot without appreciable defocusing, and thus contributed no significant error to the spot size. The combination of slow scan velocity and the relatively fast decay time of the phosphor essentially eliminated the decay tail. It was also observed that spot size varies slightly with position on the CRT for any given focus voltage. Furthermore, somewhat smaller spots are obtainable in the center of the screen than at the edge. Small spots are of greatest importance at the origin, so the focus is set at the optimum for that point, and the spot size elsewhere is satisfactory.

Phosphor decay time to 50 percent was found by varying the scan velocity and measuring the resulting spot sizes by slit scanning. A graph of the results is shown in figure 9. It is noted that the curve approaches a straight line at high scan velocities. The slope of this linear portion of the curve is the decay time to 50 percent and is 0.8 microsecond. If the decay characteristic is a simple single-component exponential, the decay time to $1/e_n$ is 1.15 microseconds (0.8/ln 2).

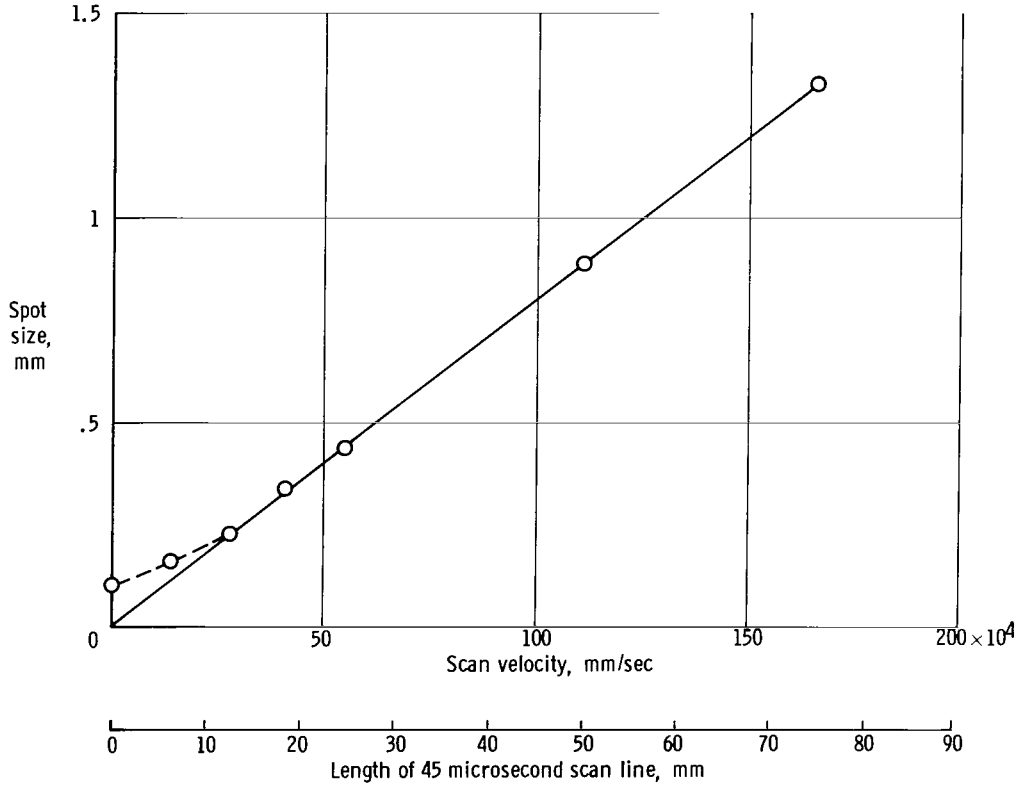

Figure 9.– Spot size versus scan velocity.

Phosphor noise for a given screen varies inversely with spot size. This variation is easily seen because a smaller spot is more greatly affected by a small imperfection in the screen than a large spot. The same experimental setup used to measure light output as a function of scan-line length was used to observe phosphor noise. Effective spot size increases with scan velocity as a result of the lengthening decay tail, and the phosphor noise reduces accordingly. Table II lists various scan velocities, associated scan-line lengths and total spot sizes, and peak-to-peak phosphor noise as a percentage

of the average signal level.

TABLE II. – EFFECT OF SCAN VELOCITY ON PHOSPHOR NOISE

Scan speed, mm/sec	Scan-line length, mm	Total spot size, mm	Phosphor noise, peak-to-peak amplitude as a percentage of average signal level
7,500	0.38	0.10	25
56,000	2.5	.15	20
560,000	25	.44	5
1,700,000	77	1.35	Negligible

Optics

Figure 10 shows the basic optical components used in the FSS and a schematic ray trace. The important characteristics of the relay lens are relative aperture, on-center modulation transfer function, and transmission efficiency both on center and at the edge of the field. The lens used in this FSS is a high-quality camera lens with an aperture of f/2.8 and a focal length of 150 millimeters. It is operated at a magnification of 0.9. The object plane has a radius of 94 millimeters. With the CRT spot positioned at the maximum radius, the transmission through the lens is about 65 percent of the transmission on center. This measurement was easily made by scanning the CRT with a uniform raster 94 millimeters in height, placing a photomultiplier on the optical axis near the first image plane, and reading the output level. The photomultiplier was then moved to a point near the edge of the first image plane, and the output read once more. The ratio of the outputs gives the relative transmission between the center and the edge of the field.

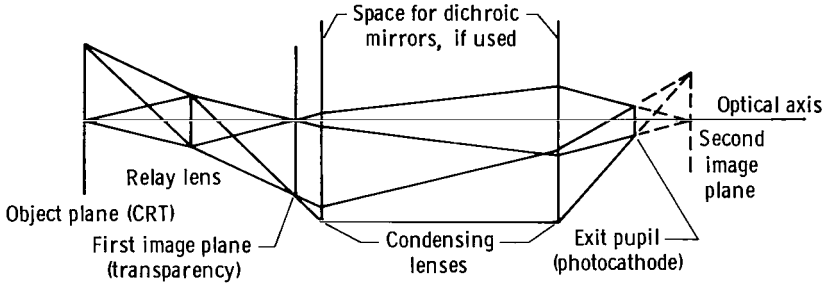

Figure 10.– Flying-spot scanner optical components.

In order to measure the absolute transmission efficiency on center, it was necessary to construct a clear aperture subtending the same solid angle as the lens at its operating distance. The ratio of the diameter of the aperture to its distance from the CRT is 1/5.9. An appropriate aperture (f/5.9) was constructed and properly placed. The light transmitted through the aperture was compared with the light transmitted through the lens on center by comparing photomultiplier outputs. This test yielded an efficiency of 80 percent.

A test was devised that would yield a segment of the on-center modulation transfer function for the lens. The setup shown in figure 11 was used. A small test pattern similar to that shown in figure 12 was scanned in both image planes. Figure 13 shows

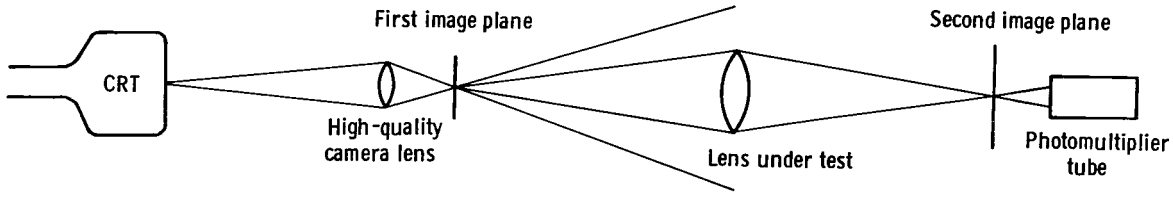

Figure 11.– Test setup for measuring the modulation transfer function of a lens.

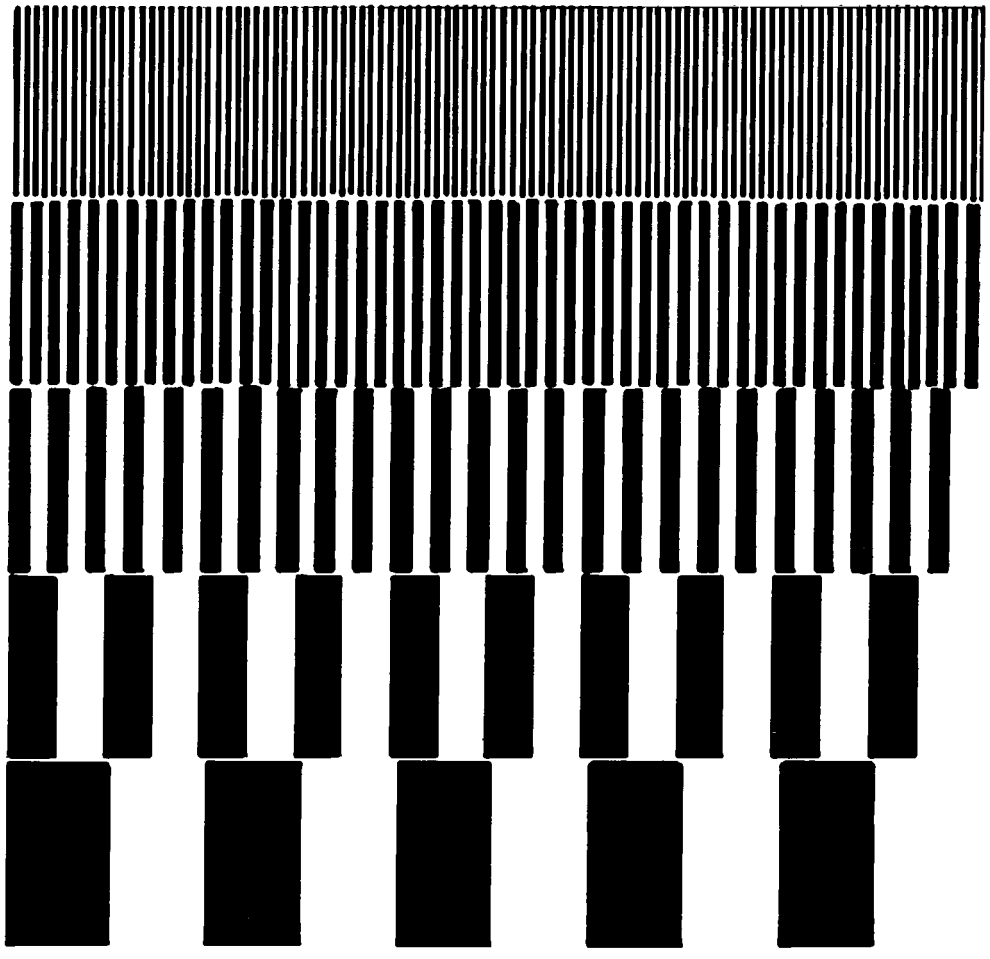

Figure 12.– Test pattern.

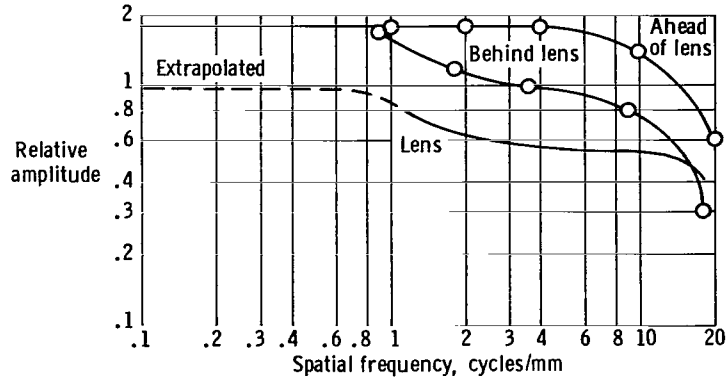

Figure 13.– Modulation transfer function.

the results obtained ahead of and behind the lens being tested. Each indicated data point was found from a particular set of bars on the test pattern. The attenuation observed between the two curves is due to the lens transfer function, which is also plotted in figure 13. Because of the magnification factor, the actual response at the second image plane was shifted to the left on the spatial frequency axis by the amount of the magnification, 0.9. The modulation transfer function is thus referred to the object, or CRT, plane. The scanning raster in both image planes was inspected by using a microscope, and scattering of light (possibly a halo) was observed in the second image plane. This observation tends to agree with the modulation transfer-function curve.

Figure 10 shows that the function of the condensing lenses is to form an exit pupil no larger than the diameter of the photocathode of the photomultiplier tube. The only parameter of interest for this portion of the optical system is the transmission efficiency both on axis and at the edge of the field. Since it was easier to measure these quantities for the entire optical system, the transmission efficiency for the whole assembly was found by comparing the light output from a uniform raster 94 millimeters in height through an f/5.9 clear aperture with the light from the same raster measured at the exit pupil. Since the uniform raster covered the field of 94-millimeter radius, relative efficiency between center and edge was obtained simply by comparing first and last scan lines. The efficiency data are summarized in table III.

TABLE III. – SUMMARY OF LENS-EFFICIENCY DATA

	Absolute efficiency on axis, percent	Absolute efficiency at edge of field, percent
Relay lens	80	50
Entire optical system	20	10
Condensing lenses (calculated from above data)	25	20

Transparencies

The scale factor of the color transparency in the FSS is 1/60,000. Little testing was performed on the transparency. A microscopic examination revealed no detail smaller than about 0.15 millimeter. Furthermore, the average transmission of the film is about 0.15 or less over most of the area. However, the lightest areas have transmissions of up to 0.5. The transparencies are in the form of film sandwiched between two glass plates.

Photomultiplier Tubes

According to the manufacturer's data, the photomultiplier tube, which was originally used in the red channel before the monochrome conversion, has an S-20 spectral response and a median photocathode sensitivity of 150 microamperes/lumen. It has a 42-millimeter diameter photocathode and a 2.8-nanosecond anode pulse rise time. This tube was used for all tests because it was the best available.

A sensitivity test was conducted by placing the photomultiplier tube behind an f/5.6 clear aperture which was exposed to the CRT. A uniform raster with an area of 25.2 centimeters^2 and a duty cycle of 0.68 was generated. The brightness of the raster was 0.0068 candela/centimeter^2 as measured with an eye-corrected photometer. For this situation, the efficiency of the aperture is unity and the magnification is infinite. The spectral correction factor is 0.87. Appendix C shows that

$$i_k = \frac{S_k g B_r A_r \pi K}{4dN^2 (1 + \frac{1}{M})^2} \tag{4}$$

$$= 0.82 \text{ microampere}$$

The photocathode actually produced 1.3 microamperes. Agreement between the calculated and measured currents is considered reasonably good for the following reasons: The brightness meter has a 20-percent tolerance; the actual photocathode sensitivity is not known; and the spectral correction factor is subject to a considerable variation.

The 2.8-nanosecond anode pulse rise time is fast enough to justify ignoring any frequency attenuation in the photomultiplier tube.

Video Amplifier

The primary feature of the video amplifier pertinent to this study is the transfer function designed to extract the maximum information from the output signal of the photomultiplier. This amplifier contains two correction stages. One is intended to be a spot-size corrector and produces high gain at high frequency with zero phase angle. A similar type of signal processing is described in reference 4. The other stage is an ordinary differentiator similar to the type described in reference 5, which produces high gain at high frequencies with appropriate phase lead. This stage is designed to

correct for the effects of phosphor decay. The amount of both types of correction is manually adjustable.

VIDEO SIGNAL PRODUCED BY THE TESTED FSS

This section presents the objective results of the signal-to-noise ratio and frequency calculations. Subjective comments about the general appearance of a picture produced by this video signal are included.

Objective Evaluation

Signal-to-noise ratio. – The signal-to-noise ratio at the photomultiplier output is computed by using equation (1), but with the factor $\frac{B_r A_r}{d}$ replaced with the luminous intensity I. Since the optical efficiency on axis is double that at the edge of the field and short scan lines (which occur near the optical axis) produce about half the light of long lines (which occur near the edge of the field), there is a cancellation of these effects. Therefore, the signal level remains constant over the field, and only one calculation is necessary. The shortest scan line is chosen. The appropriate numbers are as follows:

$N = 2.8$

$M = 0.9$

$S_k = 150 \times 10^{-6}$ ampere/lumen

$K = 0.87$

$e = 1.6 \times 10^{-19}$ coulombs

$\Delta f = 4.2 \times 10^6$ hertz (taken for average television)

$I = 0.13$ candela

$g = 0.2$

It follows that the signal-to-noise ratio is

$$S/N = \frac{0.9}{2N(1 + \frac{1}{M})} \left(\frac{\pi S_k g I K}{2e\Delta f}\right)^{\frac{1}{2}} = 210$$

This is a very good signal-to-noise ratio for a video signal.

As shown in table II, phosphor noise can have a peak-to-peak value of up to 25 percent of the average signal level. Although this phosphor noise is high, it does diminish as the scan lines get longer. This noise is considered further in the Subjective Comments section.

Frequency content. – The frequency content of a video signal is of major importance in determining the quality of a television picture; therefore, it is necessary to translate the CRT spot size and phosphor decay time into a transfer function based on the time domain. The spatial frequency response of figure 6 is converted to time frequency response by plotting the curves on a time-based abscissa. The conversion is made by realizing that nondimensional frequency C, defined as $\frac{n\pi S}{L}$, is equal to $\frac{2\pi fS}{V}$. Also, the ratio R of decay length to spot size, defined as $\frac{D}{S}$, is equal to $\frac{t_d V}{S}$. Knowing spot size, decay time, and scan velocity, it is possible to find R and plot the transfer function G′ on a frequency abscissa. This can be done either by using equations (D1) to (D3) in appendix D or by cross-plotting from figure 6.

Using the spot size of 0.1 millimeter and the decay time of 1.15 microseconds as measured on the CRT, the time-based transfer function is shown in figure 14 for a series of scan line lengths (or scan velocities). The curves were computed from equations (D1) to (D3). An experimentally measured curve is also shown. This curve is the same as the curve labeled "Ahead of lens" in figure 13, but with the abscissa converted to time frequency and the ordinate normalized. The experimental curve was generated by using a scan line 2.5 millimeters long; it fits well between the curves computed for 1-millimeter and 5-millimeter scan lines.

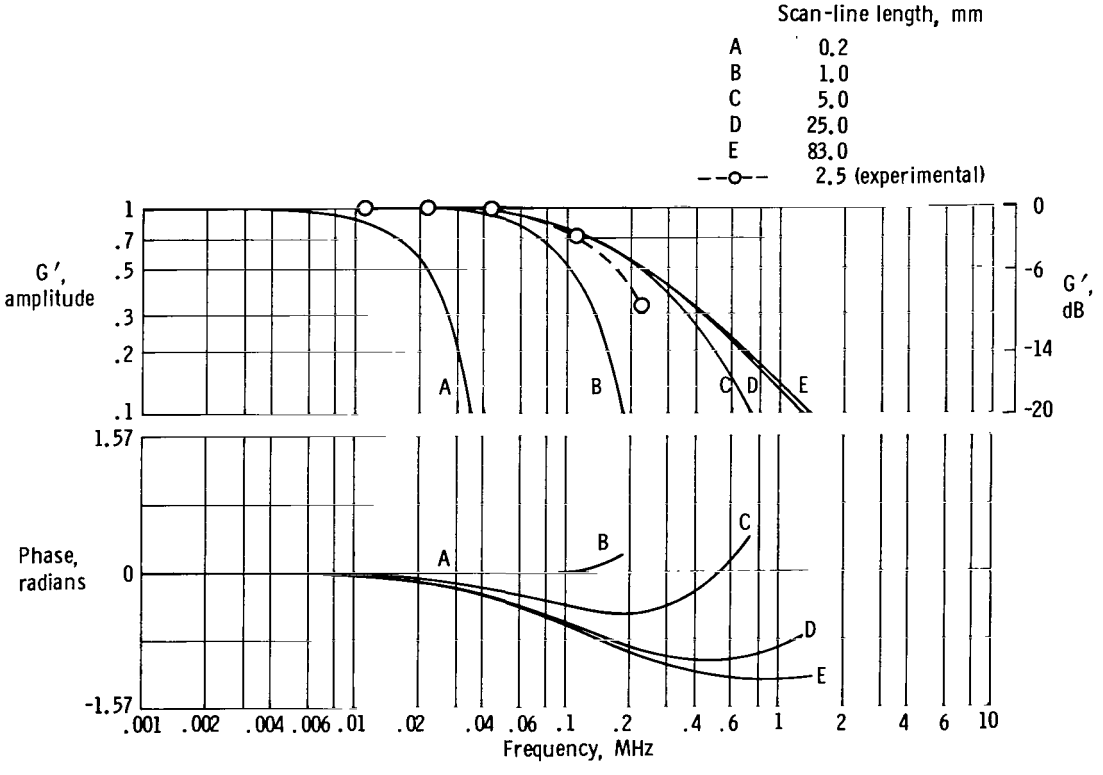

Figure 14.– Transfer admittance versus time frequency for several scan-line lengths. Scan time, 45 microseconds; phosphor decay time, 1.15 microseconds; spot size, 0.1 mm.

Several important conclusions can be drawn from figure 14. Standard 525-line television has a scan-line repetition frequency of 15,750 hertz and should operate with video containing frequencies up to roughly 4 megahertz in order to be classified as "good." This FSS is clearly unable to produce any information at frequencies approaching 4 megahertz. The worst case is the shortest scan line, which contains video frequencies only slightly above the line rate. When the modulation transfer function of the relay lens is included as shown in figure 15, the short line is still worse; it produces nothing usable. In this FSS, the raster that produces the shortest scan line simulates an aircraft altitude of 3.6 meters. However, this raster also generates longer lines, including one that is 94 millimeters long. Therefore, some information is available in the video which is obtained from longer scan lines representing detail farther from the observer's position.

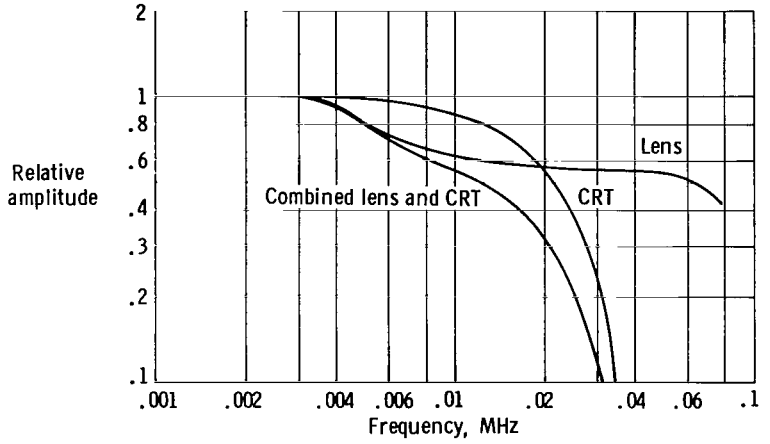

Figure 15.– Short-line transfer admittance.

As the altitude of the aircraft increases, the shortest scan line gets longer. For example, an altitude of 90 meters produces a minimum-length scan line of 5 millimeters. Neglecting the effects of the lens, this line produces a signal that contains frequencies up to 0.7 megahertz, which is a significant improvement over the lower altitude. The effects of the lens become less important as longer scan lines are considered. The longer lines mean higher scan velocities and larger effective spots because of the phosphor decay tail. Thus, the lens contributes less frequency attenuation.

The video frequency content was calculated without using either the transparency scale factor or magnification. Only the raster scale factor was used. Frequency content is not affected by magnification of the raster.

The video amplifier is supposed to amplify the high frequencies in the video; however, high-frequency amplification cannot improve the video significantly. The shorter scan lines roll off so fast that there is nothing to work with. The longer lines are already the best available and represent video that is needed least (because this information is farthest from the simulated aircraft). Furthermore, if high-frequency amplification is to be used, it should vary its bandpass to accommodate each scan-line length. Therefore, it is concluded that the video amplifier in this FSS is inadequate in its design (it has only a fixed bandpass) and performs a questionable

function. The photomultiplier tube produces no significant attenuation of these video frequencies.

Although the transparency has not been included in the FSS transfer function, it is interesting to consider the 0.15 millimeter detail size. An 0.18-millimeter scan line (0.2 millimeter at the CRT multiplied by a magnification of 0.9) cannot find much information because the scan line is only slightly longer than the size of the smallest detail.

There are several approaches that may be considered for possible improvements. Since the short-line frequency content is limited solely by CRT spot size, a smaller spot would help. However, light output, signal-to-noise ratio, and phosphor noise may approach unacceptable levels. Improvements of the order of 100 are actually required; no spot size on a CRT can even approach this. Increasing the CRT size to permit an increase in raster scale factor without loss of forward visibility would also help, but again the improvement would be very small compared to what is required. A better relay lens could produce only a very limited improvement. Using a faster decay phosphor offers no improvement of short-line video. Such a phosphor would improve the frequency content of the longer lines, but these lines are not the main problem. Light output, burn resistance, and a low-noise screen are the important phosphor characteristics. Usable video can be obtained only by staying at higher altitudes or by greatly increasing the raster scale factor with a consequent loss of forward visibility.

By carefully selecting a superior CRT with a small spot, a relay lens of very high quality, and a transparency containing very fine detail, a significant improvement may be obtainable, possibly as much as a factor of four. However, each element would have to be carefully optimized. Although such an improvement would not produce good video at an altitude of 3.6 meters, it would permit video quality at 20 meters to be as good as that available at 80 meters in the tested FSS. Video of this quality may prove to be useful in some applications.

Subjective Comments

The most important characteristic of the video produced by the FSS is best defined by answers to questions such as, "How good is the picture?" "What can it be used for?" and "What information can it present?" In order to attempt to answer such questions, it was necessary to display a picture constructed from the video signal. A high-quality monitor was used. It is assumed that the characteristics of the monitor itself did not significantly affect the subjective impression conveyed by the picture.

A number of picture characteristics deserve mention. First, the picture is quite free from random noise. A little random noise is noticeable, but is found in practically all television displays. A test showed that photomultiplier shot noise is not the cause of the observed noise. The CRT light output was reduced in successive steps, and the photomultiplier gain was simultaneously increased to compensate for the loss in signal level. The random noise in the picture did not appear to increase until the light output from the CRT approached 10 percent of its usual level.

Phosphor noise produces some interesting effects, mainly because it is not random. In a stationary picture it becomes a steady ripple superimposed over the terrain. Pitch,

altitude, and roll changes cause the ripple to continue to appear as part of the terrain, since the relative position between phosphor grains and the transparency is stationary. Heading and positional changes cause the ripple to move with the aircraft, since there is relative motion between the phosphor grains and the transparency. This noise is most noticeable in light areas on the transparency and is striking when the transparency is removed and the picture is white. However, in areas on the transparency having average density, it is not particularly objectionable. A scanner tube having a defective screen with very high phosphor noise was installed in order to observe the effect. The resultant increase in phosphor noise was highly unsatisfactory. It was concluded that the present level is near a reasonable limit. This conclusion is in accord with the information in table II, which shows a very low noise on long scan lines, which in turn generate most of the picture at moderate altitudes.

The effects of video frequency content are not as objectionable as figure 14 implies. At minimum altitude there is little to be seen at the bottom of the picture. However, in spite of the lack of detail, the outlines of the runway and the center stripes are sufficiently well defined to enable satisfactory heading, lateral drift, and relative perspective information to be obtained from the display. Figure 16 is a photograph taken at minimum altitude. Operating experience with this FSS indicates that the picture presents sufficient information to enable a flight-simulator pilot to flare his aircraft. However, touchdown cues are inadequate. Therefore, this FSS is considered to have limited value when used for landing simulations.

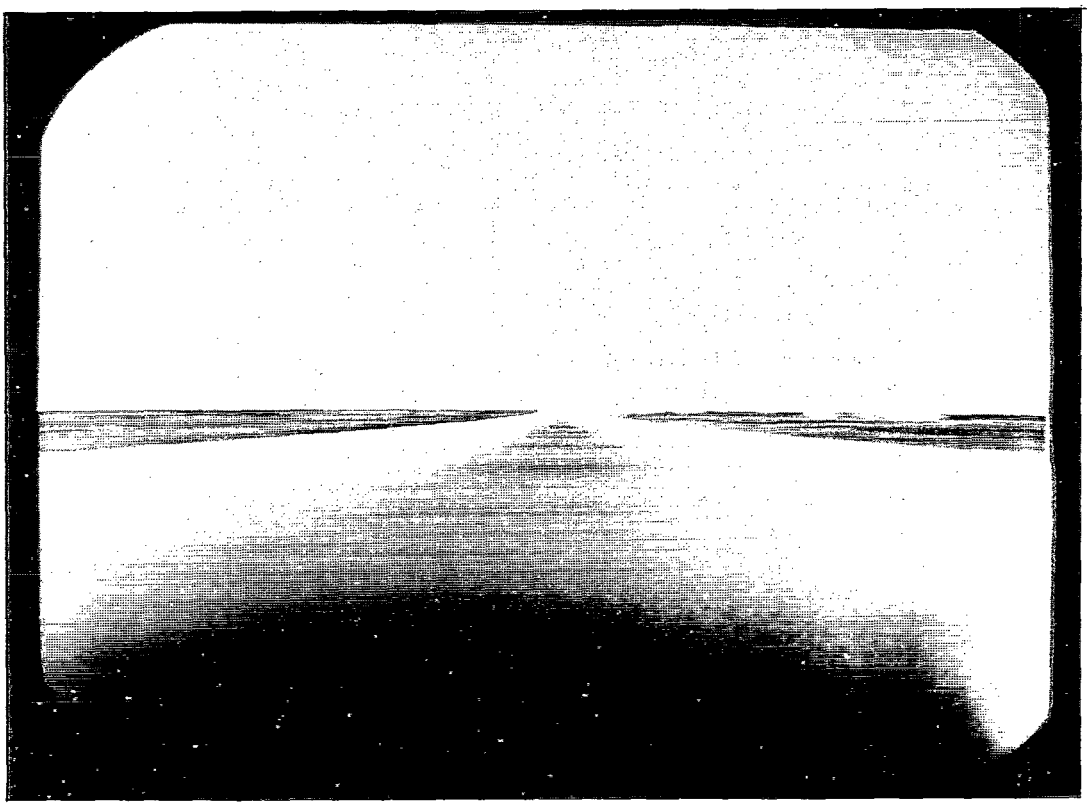

E-19439

Figure 16.– FSS picture taken at minimum altitude showing low video bandwidth in near field.

Another problem appears in the picture at low altitude, but this affects detail in the distance. Since the most distant FSS raster lines are widely spaced at low altitude, small details flicker in and out as the raster lines either cross or miss those points on the transparency. If there is a line in the picture (such as a road) which lies nearly parallel to the scan lines and intersects a few of them, it will appear as a dashed line (fig. 17), with the dashes drifting across the picture as the simulated aircraft moves forward. These effects are somewhat objectionable and distracting. This problem is discussed extensively in reference 6. There are several approaches to this problem. One is to intentionally defocus the CRT spot when the lines are widely spaced. Another is to select a relay lens that produces vertical defocusing of the spot off the optical axis. This problem requires further study.

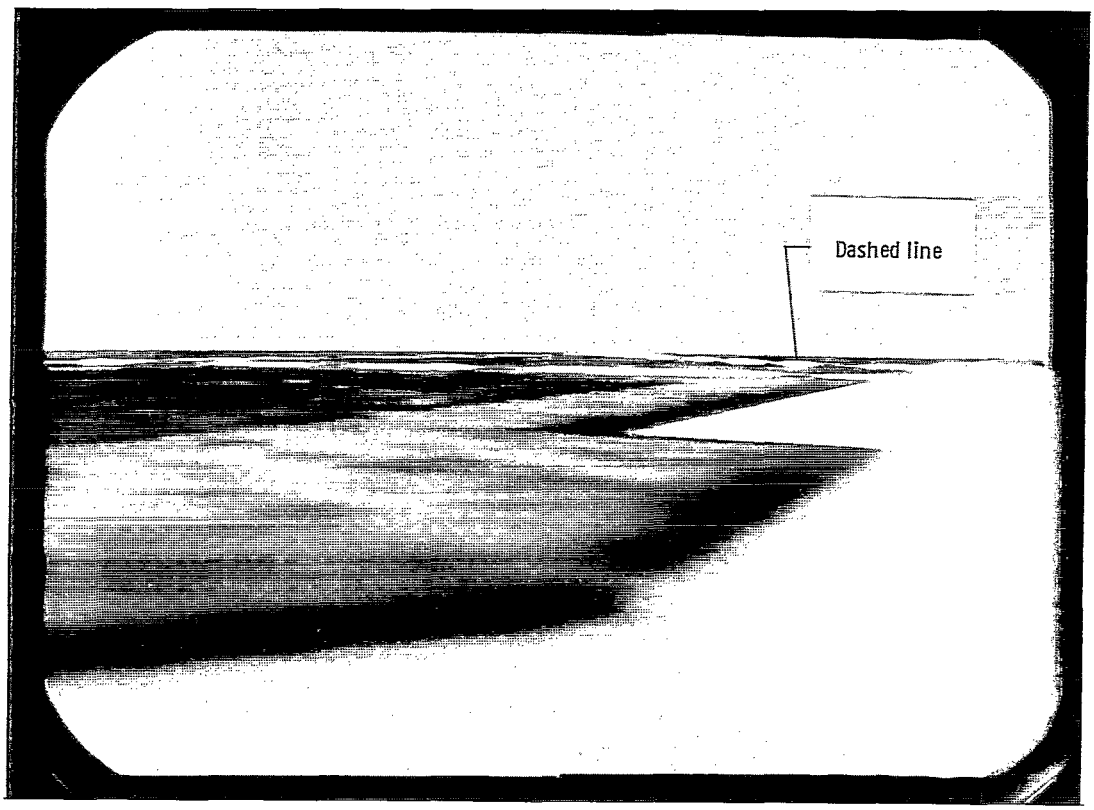

E-19442

Figure 17.– FSS picture taken at low altitude showing dashed-line effects.

Maximum altitude introduces the problem of fixed forward visibility. Figure 18 is a photograph showing the artificial haze layer which fills the gap between the horizon and the terrain. The altitude shown is 800 meters. The artificial haze appears very unrealistic. Deleting the haze layer presents a false horizon; however, it has been found that if the maximum altitude is limited to about 400 meters and the haze is deleted, the depressed horizon is not particularly objectionable. In fact, it helps to give an impression of altitude (possibly by exaggerating the effect of the earth's curvature).

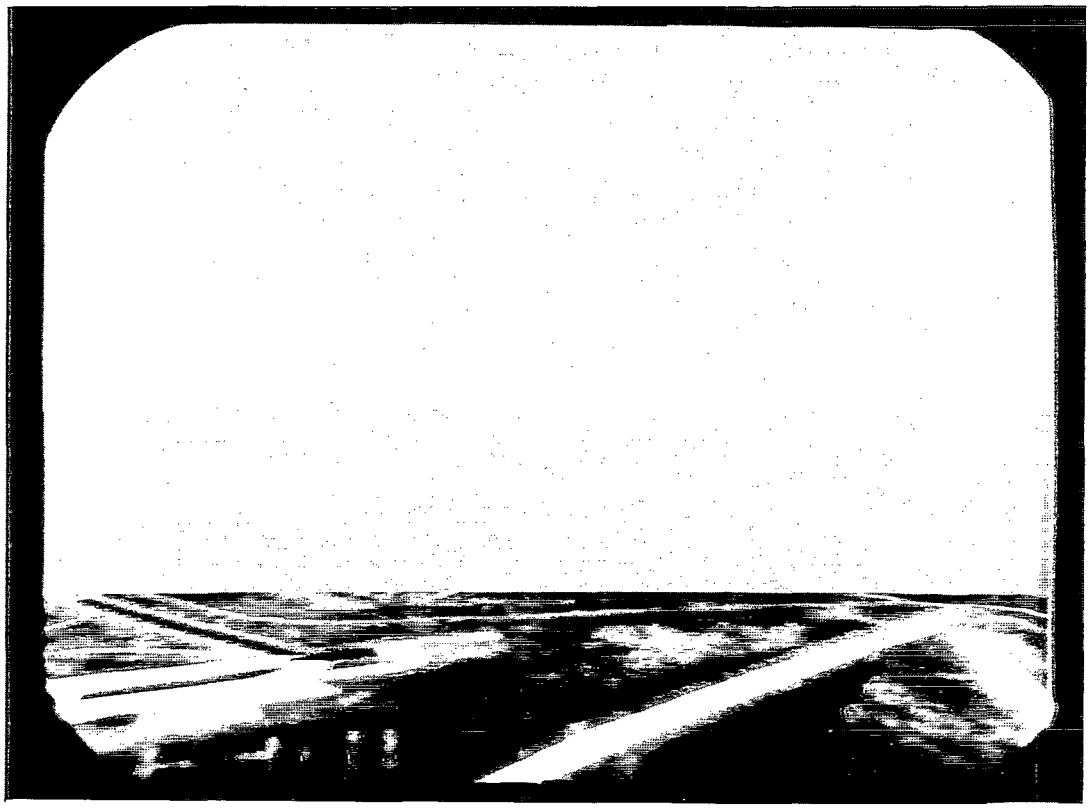

E-19443

Figure 18.– FSS picture taken at an altitude of 800 meters showing haze layer and excessive contrast.

Figure 18 also shows another problem. The white or very light detail appears too bright in comparison to the surrounding terrain. The excessive brightness is attributed to the fact that the transmission of the transparency ranges from high to very low. A more suitable transparency for this application should have relatively high transmission over all the area, with an "average" of approximately 0.5. Maximum transmission should be near unity, and minimum transmission should not be less than 0.1. This range of transmission corresponds to a film density range of 0 to 1. Higher densities are common in good photographic transparencies, but details in areas of density greater than 1 appear black to the FSS. If the gain is turned up to detect these details, the white areas saturate the picture. A nonlinear amplifier may be able to compensate partially for this effect, but limiting the FSS to the lowest 10 percent of its range most of the time can only reduce the signal-to-noise ratio otherwise available.

With the FSS tested, relatively good pictures with no particular defects are available over an altitude range of approximately 80 meters to 400 meters. Figure 19 shows a scene at a moderate altitude. The user must decide how much picture degradation can be accepted in return for a greater altitude range. It is also necessary to emphasize that altitude ranges other than those described are immediately obtainable by merely changing the transparency scale factor. If, for example, a transparency having a 1/300,000 scale were used, good pictures would be available between 400 meters and 2000 meters altitude and forward visibility would increase to 22 kilometers. A

ratio defining the proportions between minimum altitude, maximum altitude, and forward visibility for good pictures might be defined as 1:5:55. Usable pictures are available outside this range, depending on the particular requirement.

E-19445

Figure 19.– FSS picture taken at moderate altitude showing relatively good performance.

Further extensions of the "good" altitude range may be possible by using various approaches. Improved FSS components may help, as discussed previously. It may be possible to increase the maximum altitude without a haze presentation by subtracting some fraction of the altitude from the pitch angle. Thus, terrain would be presented most of the way to the correct horizon position at all times, but the pitch presentation would be incorrect. Further study is required to determine how much, if any, of this sort of compensation could be tolerated. Still other possibilities exist that may be capable of extending the useful altitude range to lower altitudes for a given scale factor while maintaining a crisp display. Since very little actual detail is present in the near field at low altitudes, an electronically generated video signal referenced to the coarse information in the scanner output (such as runway outline) might improve the display. Such a signal would have to be generated in a nonlinear fashion. Furthermore, it may be capable only of sharpening the existing picture without adding any information. Such a study would require a nonlinear analysis of the scanning system, which may be possible if an analog computer is used in the manner described in appendix E.

CONCLUDING REMARKS

An analysis has been made of the flying-spot scanner (FSS) used as a television video signal generator for visual flight simulation. It was found that the FSS is a relatively simple, low-cost device that can simulate all degrees of freedom of an aircraft except roll. The simulated motions are capable of large excursions at high rates and are independently variable. A variety of terrain segments can be simulated easily by appropriate transparencies. The transparencies can be interchanged as rapidly as required.

The FSS technique introduces some limitations, such as a fixed upper limit on forward visibility and an inability to simulate three-dimensional terrain. Field of view was found to be limited to about 1 radian vertically and horizontally. In order to analyze the video signal, equations were derived to compute its frequency content and signal-to-noise ratio.

A commercially available FSS was tested and analyzed. The video signal produced by this FSS is free of excessive random noise. The frequency content of the video signal is particularly poor at very low altitudes but better at higher altitudes. Improved components were found to be capable of improving the low-altitude video somewhat, but not enough for the video performance to be considered good.

The tested FSS was found to be capable of producing acceptable pictures over an altitude range of 5 to 1. Several approaches are discussed which may be capable of extending this altitude range. These approaches require further study.

Flight Research Center,
National Aeronautics and Space Administration,
Edwards, Calif., December 31, 1968,
125-19-06-03-24.

APPENDIX A

DERIVATION OF RASTER EQUATIONS

In order to properly shape a raster on a scanner tube, it is necessary to compute the position B (fig. A-1) of a point on the ground as a function of its position D on a vertical window in front of the observer O′ when O′, D, and B are collinear. Point D

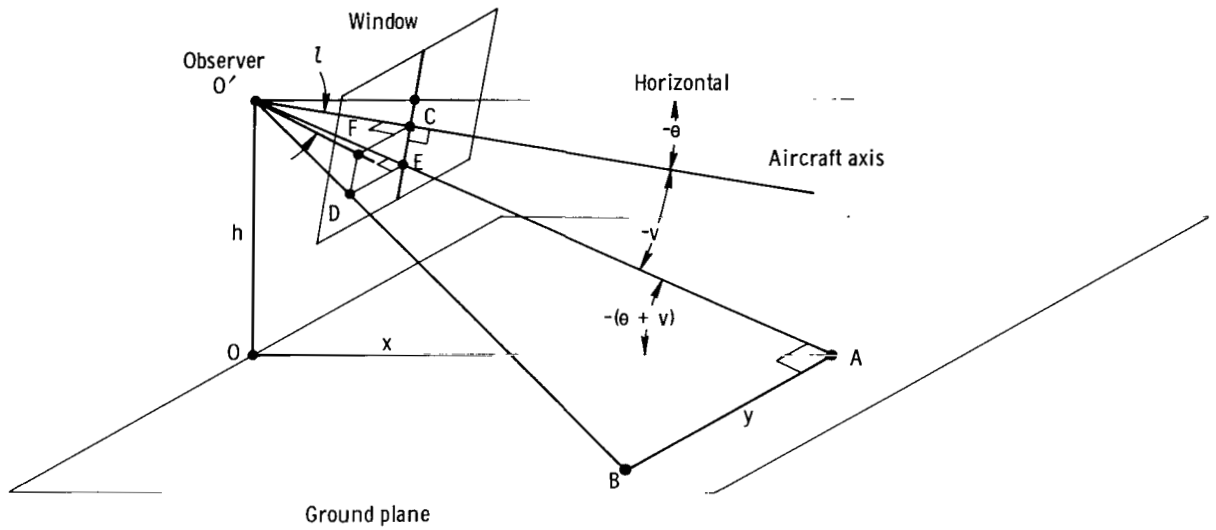

Figure A-1.– Location of a point on the ground as a function of altitude, pitch angle, and the angular coordinates of a point on a window.

corresponds to the position of the scanning spot on the television display raster, while point B corresponds to the position of the scanning spot on the FSS raster. In this derivation, the notation $\overline{AB}$ is defined as the distance between points A and B. This notation does not imply a vector. Assuming the observer is at altitude h and pitch angle θ (θ is negative downward), it is seen that

$$\overline{OA} = -\overline{OO'} \cot(\theta + v) \tag{A1}$$

$$\overline{AB} = \frac{\overline{O'A} \times \overline{DE}}{\overline{O'E}} \tag{A2}$$

$$\overline{O'A} = -\overline{OO'} \csc(\theta + v) \tag{A3}$$

$$\overline{DE} = \overline{FC} \tag{A4}$$

$$\overline{FC} = \overline{O'C} \tan l \tag{A5}$$

$$\overline{O'C} = \overline{O'E} \cos v \tag{A6}$$

Combining equations (A2) to (A6) yields the expression

$$\overline{AB} = - \overline{OO'} \tan l \cos v \csc (\theta + v)$$

Letting $\overline{OA} = x$, $\overline{AB} = y$, and $\overline{OO'} = h$, it follows that

$$y = -h \tan l \cos v \csc (\theta + v) = \frac{-h \tan l}{\tan v \cos \theta + \sin \theta} \tag{A7}$$

$$x = -h \cot (\theta + v) = \frac{-h(1 - \tan \theta \tan v)}{\tan \theta + \tan v} \tag{A8}$$

Thus, the coordinates of point B are computed in terms of the aircraft altitude h and pitch angle θ, as well as the angular coordinates of point D with respect to point C. The spot position on the display raster determines l and v when the distance between the observer and the display screen are known. The angles can be computed from the following equations:

$$\frac{\overline{FC}}{\overline{O'C}} = \tan l$$

$$\frac{\overline{EC}}{\overline{O'C}} = - \tan v$$

For a given viewing position, $\overline{O'C}$ is constant and $\overline{EC}$ and $\overline{FC}$ change at constant rates, since the television display scan moves at a constant velocity in both the vertical and horizontal directions. Therefore, tan l and - tan v become proportional to the instantaneous horizontal and vertical coordinates of the scanning spot on the television display raster. These coordinates are frequently referred to as the horizontal sawtooth and the vertical sawtooth, because they vary in sawtooth fashion and have repetition rates of the television line rate and field rate, respectively. The observer's horizontal and vertical fields of view are $2l_{max}$ and $2v_{max}$.

The sides of the raster where $y = y_{max}$ are found by setting $l = l_{max}$ in equation (A7) and eliminating tan v between equations (A7) and (A8) in the following manner:

$$y_{max} = \frac{-h \tan l_{max}}{\tan v \cos \theta + \sin \theta}$$

$$\tan v = -\frac{h \tan l_{max}}{y_{max} \cos \theta} - \tan \theta = \frac{h + x \tan \theta}{h \tan \theta - x}$$

Solving for y_{max}

$$y_{max} = \tan l_{max}(x \cos \theta - h \sin \theta) \tag{A9}$$

This is a linear relationship for any given value of θ, h, and l_{max}.

For a pitch angle of zero, the length of the shortest scan line becomes

$$2y_{max} = \frac{2h \tan l_{max}}{\tan v_{max}} \tag{A10}$$

since $-v_{max}$ is the vertical viewing angle of the shortest scan line.

APPENDIX B

DERIVATION AND COMPUTATION OF SPECTRAL CORRECTION FACTOR

The light output from a cathode-ray tube phosphor source is easily measured with an eye-corrected photometer. A spectral correction factor will determine the relative amount of this light that represents excitation to a photocathode. The sensitivity of the photocathode is assumed to be calibrated in terms of light from a blackbody source at 2870° K. The following definitions apply:

$S(\lambda)$ relative sensitivity of a photocathode as a function of wavelength of light

$E(\lambda)$ relative sensitivity of standard human eye as a function of wavelength of light

$P(\lambda)$ relative spectral-power distribution of a glowing phosphor as a function of wavelength of light

$B(\lambda)$ relative spectral-power distribution of a radiating blackbody at 2870° K as a function of wavelength of light

If a blackbody source and a phosphor source are adjusted to provide equal amounts of light in terms of eye response, the spectral correction factor will be the ratio of the output of the photocathode looking at the phosphor source to its output looking at the blackbody source. The response of the photocathode to any source requires a knowledge of its absolute sensitivity over the spectrum as well as the emission power of the source over the spectrum. However, by introducing a normalizing factor and using the relative spectral values, the spectral correction factor becomes

$$K = \text{normalizing factor} \times \frac{\int_0^\infty S(\lambda)P(\lambda)\,d\lambda}{\int_0^\infty S(\lambda)B(\lambda)\,d\lambda}$$

The normalizing factor is equal to the relative response of the eye to the blackbody divided by the relative response of the eye to the phosphor. The result is

$$K = \frac{\int_0^\infty E(\lambda)B(\lambda)\,d\lambda}{\int_0^\infty E(\lambda)P(\lambda)\,d\lambda} \times \frac{\int_0^\infty S(\lambda)P(\lambda)\,d\lambda}{\int_0^\infty S(\lambda)B(\lambda)\,d\lambda} \tag{B1}$$

This expression is completely independent of the amplitude of any of the spectral curves required to compute it. All amplitude factors appear in the numerator and denominator, and they cancel out.

APPENDIX B

Several spectral correction factors were computed by making some relatively coarse approximations to the spectral emission characteristics of several CRT phosphors and the response characteristics of the human eye and an S-20 photocathode. Phosphors of the same type vary in their characteristics from sample to sample, and photocathodes of the same type also vary. Furthermore, "eye corrected" photometers do not exactly match the characteristics of the "standard" eye. Thus, the use of only a rough approximation seems justified for this type of calculation. It must be recognized, therefore, that actual measurements may vary considerably from those predicted by the calculations.

Figure B-1 shows the approximations used for the emission spectrum of a blackbody at 2870° K and the responses of the eye and an S-20 photocathode with ordinates normalized. Figure B-2 shows the approximations used for the emission spectra of five phosphors, where the ordinates are the same as for figure B-1. The dashed portions of the eye curve and the P-16 curve were used to obtain a more realistic response of the eye to the P-16 phosphor.

Inasmuch as a large number of similar computations is required, only the following sample is shown:

$$\int_0^{\infty} S(\lambda)B(\lambda)\,d\lambda = \int_{400}^{440} \left(\frac{\lambda - 400}{400}\right) d\lambda + \int_{440}^{800} \left(\frac{\lambda - 400}{400}\right)\left(\frac{800 - \lambda}{360}\right) d\lambda \approx 74$$

Table I (page 10) shows the results for the five phosphors.

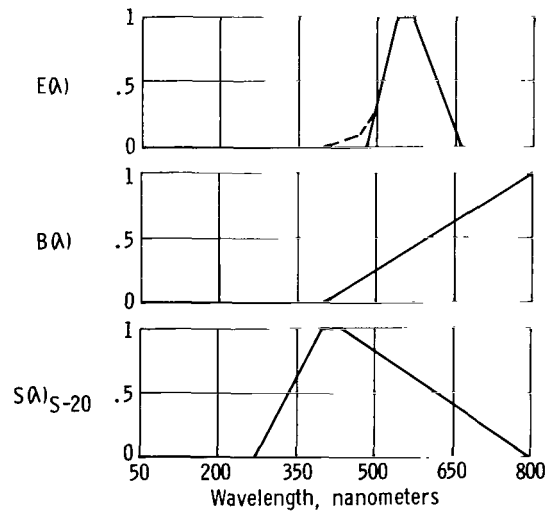

Figure B-1.– Approximations of the emission spectrum of a blackbody at 2870° K and the spectral response of the human eye and an S-20 photocathode.

APPENDIX B

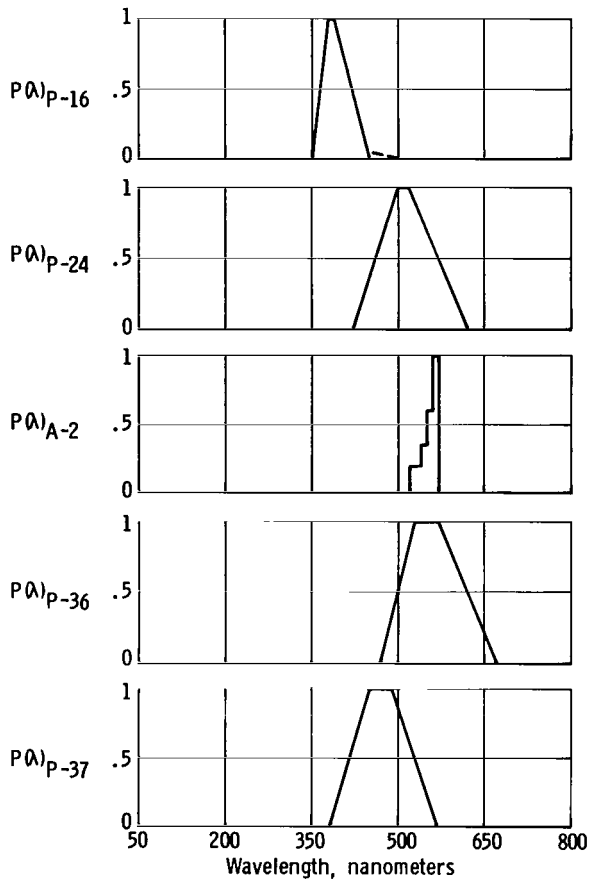

Figure B-2.– Approximations of the emission spectra of several CRT phosphors.

APPENDIX C

DETERMINATION OF SIGNAL-TO-NOISE RATIO

The maximum signal-to-noise ratio obtainable from a flying-spot scanner is the signal-to-noise ratio of the output of the photomultiplier tube. Photomultiplier noise theory indicates that the primary noise source in the tube is the shot noise from photocathode emission. Dynode multiplication increases this noise roughly 10 percent or 20 percent over the signal ranges of interest for scanners. The governing equation is

$$S/N = 0.9\sqrt{\frac{i_k}{2e\Delta f}} \tag{C1}$$

where

S/N	voltage (or current) signal-to-noise ratio
0.9	approximate S/N reduction due to dynode noise
i_k	photocathode current, amperes
e	electronic charge (approximately 1.6×10^{-19} coulombs)
Δf	bandwidth, hertz

The amount of cathode current is proportional to the amount of light falling on the photocathode. Hence

$$i_k = S_k F K \tag{C2}$$

where

S_k	photocathode sensitivity, amperes per lumen
F	luminous flux, lumens
K	spectral correction factor

The luminous flux F depends on the size of the spot on the cathode-ray tube, its brightness, the solid angle and efficiency of the optical system, and the transmission of the transparency. For a white bit of detail, the transmission of the transparency is near unity, and this is used for signal-to-noise computations. Fundamental optical principles yield the following equations:

$$F = gB_S A_S \psi \tag{C3}$$

$$\psi = \frac{\pi}{4N^2\left(1 + \frac{1}{M}\right)^2} \tag{C4}$$

where

g	transmission efficiency of optical system
B_S	average brightness of CRT spot
A_S	surface area of spot
ψ	solid angle subtended by optical system
N	relative aperture of optical system
M	magnification of optical system

It is difficult to measure directly either the peak or the average brightness of a CRT spot, and some doubt may exist regarding its effective area. Therefore, the product $B_S A_S$ in equation (C3) is replaced by the following expression:

$$B_S A_S = \frac{B_r A_r}{d} \tag{C5}$$

where

A_r	actual area of a uniform raster
B_r	average brightness of the raster
d	duty cycle of raster

Finally, combining equations (C1) to (C5) yields the expressions

$$S/N = \frac{0.9}{2N(1 + \frac{1}{M})} \left(\frac{\pi S_k g B_r A_r K}{2ed\Delta f} \right)^{\frac{1}{2}} \tag{1}$$

and

$$i_k = \frac{S_k g B_r A_r \pi K}{4dN^2 (1 + \frac{1}{M})^2} \tag{4}$$

APPENDIX D

COMPUTATION OF SCANNING TRANSFER FUNCTION

The spatial frequency response (transfer function) of a scanning spot can be computed from the spot profile. It is first necessary to find Z_1 (shown in fig. 5) as a function of S and D. The criterion for Z_1 is that $\left.\frac{dT(Z)}{dZ}\right|_{Z=Z_1}$ is the same for both the exponential and cosine portions of the curve, and the curve is continuous. The two parts of the curve are defined as

$$T_c(Z) = 1 + \cos\left(\frac{\pi Z}{S}\right)$$

and

$$T_e(Z) = \left[1 + \cos\left(\frac{\pi Z_1}{S}\right)\right] \exp\left(\frac{Z - Z_1}{D}\right)$$

The derivatives are

$$\left.\frac{dT_c(Z)}{dZ}\right|_{Z=Z_1} = -\frac{\pi}{S} \sin\left(\frac{\pi Z_1}{S}\right)$$

and

$$\left.\frac{dT_e(Z)}{dZ}\right|_{Z=Z_1} = \frac{1 + \cos\left(\frac{\pi Z_1}{S}\right)}{D}$$

When the derivatives are equal,

$$1 + \cos\left(\frac{\pi Z_1}{S}\right) = -\pi\frac{D}{S} \sin\left(\frac{\pi Z_1}{S}\right)$$

Rearranging yields

$$\frac{\sin\left(\frac{\pi Z_1}{S}\right)}{1 + \cos\left(\frac{\pi Z_1}{S}\right)} = -\frac{S}{\pi D} = \tan\left(\frac{\pi Z_1}{2S}\right)$$

Therefore

$$Z_1 = -\frac{2S}{\pi} \tan^{-1}\left(\frac{S}{\pi D}\right)$$

APPENDIX D

The equation for the transfer function presented in reference 3 (which is the Fourier transform of the aperture) is

$$Y(n) = \int_{\text{aperture}} T(Z) \exp\left(\frac{i\pi nZ}{L}\right) dZ$$

where

$Y(n)$	equivalent transfer admittance
Z	dimension in direction of scan (called ξ in ref. 3)
$T(Z)$	intensity profile of scanning spot
n	number of complete cycles in a scan line
L	half the length of the scan line
$\frac{n\pi}{L}$	radian frequency per unit length

Substituting for $T(Z)$ yields

$$Y(n) = \int_{-\infty}^{Z_1} \left[1 + \cos\left(\frac{\pi Z_1}{S}\right)\right] \exp\left(\frac{Z - Z_1}{D}\right) \exp\left(\frac{i\pi nZ}{L}\right) dZ + \int_{Z_1}^{S} \left[1 + \cos\left(\frac{\pi Z}{S}\right)\right] \exp\left(\frac{i\pi nZ}{L}\right) dZ$$

Calling the first integral I_1 and the second integral I_2, the following substitutions are made:

$$Q = \frac{Z_1}{S}$$

$$R = \frac{D}{S}$$

$$C = \frac{n\pi S}{L}$$

$$I_1 = \int_{-\infty}^{SQ} [1 + \cos(\pi Q)] \exp\left(\frac{Z - SQ}{SR}\right) \exp\left(\frac{iCZ}{S}\right) dZ$$

$$I_2 = \int_{SQ}^{S} \left[1 + \cos\left(\frac{\pi Z}{S}\right)\right] \exp\left(\frac{iCZ}{S}\right) dZ$$

The details of integration are carried out as follows:

APPENDIX D

$$I_1 = [1 + \cos(\pi Q)] \int_{-\infty}^{SQ} \exp\left[Z\left(\frac{1}{SR} + \frac{iC}{S}\right) - \frac{Q}{R}\right] dZ = [1 + \cos(\pi Q)] \left.\frac{\exp\left[Z\left(\frac{1}{SR} + \frac{iC}{S}\right) - \frac{Q}{R}\right]}{\frac{1}{SR} + \frac{iC}{S}}\right|_{-\infty}^{SQ}$$

$$= \frac{SR\,[1 + \cos(\pi Q)]\,\exp(iQC)}{1 + iRC} = \frac{SR[1 + \cos(\pi Q)](1 - iRC)\exp(iQC)}{1 + R^2C^2}$$

$$I_1 = \frac{SR[1 + \cos(\pi Q)]}{1 + R^2C^2} \left\{\cos(QC) + RC \sin(QC) - i\,[RC \cos(QC) - \sin(QC)]\right\}$$

$$I_2 = \int_{SQ}^{S} \left[1 + \cos\left(\frac{\pi Z}{S}\right)\right]\left[\cos\left(\frac{CZ}{S}\right) + i \sin\left(\frac{CZ}{S}\right)\right] dZ$$

$$= \int_{SQ}^{S} \cos\left(\frac{CZ}{S}\right) dZ + i \int_{SQ}^{S} \sin\left(\frac{CZ}{S}\right) dZ + \frac{1}{2} \int_{SQ}^{S} \left[\exp\left(\frac{i\pi Z}{S}\right) + \exp\left(\frac{-i\pi Z}{S}\right)\right] \exp\left(\frac{iCZ}{S}\right) dZ$$

$$= \frac{S}{C} \sin\left(\frac{CZ}{S}\right)\Bigg|_{SQ}^{S} - i\frac{S}{C} \cos\left(\frac{CZ}{S}\right)\Bigg|_{SQ}^{S} + \frac{1}{2} \int_{SQ}^{S} \exp\left[Z\left(\frac{iC}{S} + \frac{i\pi}{S}\right)\right] dZ + \frac{1}{2} \int_{SQ}^{S} \exp\left[Z\left(\frac{iC}{S} - \frac{i\pi}{S}\right)\right] dZ$$

$$= \frac{S}{C}\,[\sin C - \sin(QC)] - i\frac{S}{C}\,[\cos C - \cos(QC)] + \frac{1}{2} \left.\frac{\exp\left[Z\left(\frac{iC}{S} + \frac{i\pi}{S}\right)\right]}{\frac{iC}{S} + \frac{i\pi}{S}}\right|_{SQ}^{S} + \frac{1}{2} \left.\frac{\exp\left[Z\left(\frac{iC}{S} - \frac{i\pi}{S}\right)\right]}{\frac{iC}{S} - \frac{i\pi}{S}}\right|_{SQ}^{S}$$

$$= \frac{S}{C}\,[\sin C - \sin(QC)] - i\frac{S}{C}\,[\cos C - \cos(QC)] + \frac{S}{2} \frac{\exp[i(C + \pi)] - \exp[i(QC + Q\pi)]}{i(C + \pi)}$$

$$+ \frac{S}{2} \frac{\exp[i(C - \pi)] - \exp[i(QC - Q\pi)]}{i(C - \pi)}$$

Substituting circular functions for the exponential functions results in

$$I_2 = S\left[\frac{\sin C - \sin(QC)}{C} + \frac{\sin(C+\pi) - \sin(QC+Q\pi)}{2(C+\pi)} + \frac{\sin(C-\pi) - \sin(QC-Q\pi)}{2(C-\pi)}\right]$$

$$- iS\left[\frac{\cos C - \cos(QC)}{C} + \frac{\cos(C+\pi) - \cos(QC+Q\pi)}{2(C+\pi)} + \frac{\cos(C-\pi) - \cos(QC-Q\pi)}{2(C-\pi)}\right]$$

Substituting G for $\frac{Y(n)}{2S}$, combining the expressions for I_1 and I_2, and rearranging further yields

$$G = \frac{1}{2}\left[\frac{\sin C - \sin(QC)}{C} - \frac{\sin C + \sin(QC+Q\pi)}{2(C+\pi)} - \frac{\sin C + \sin(QC-Q\pi)}{2(C-\pi)}\right]$$

$$+ \frac{R}{2}\left[\frac{1+\cos(\pi Q)}{1+R^2C^2}\right]\left[\cos(QC) + RC\sin(QC)\right]$$

$$- \frac{i}{2}\left[\frac{\cos C - \cos(QC)}{C} - \frac{\cos C + \cos(QC+Q\pi)}{2(C+\pi)} - \frac{\cos C + \cos(QC-Q\pi)}{2(C-\pi)}\right]$$

$$- i\frac{R}{2}\left[\frac{1+\cos(\pi Q)}{1+R^2C^2}\right]\left[RC\cos(QC) - \sin(QC)\right] \qquad \text{(D1)}$$

Normalizing G requires finding the magnitude of G for $C = 0$, which is

$$|G|_{c=0} = \frac{1}{2}\left[1 - Q - \frac{\sin(\pi Q)}{\pi}\right] + \frac{R}{2}\left[1 + \cos(\pi Q)\right] \qquad \text{(D2)}$$

Finally, the desired transfer function becomes

$$G' = G/|G|_{c=0} \qquad \text{(D3)}$$

The limit of equation (D3) as R tends to zero is as follows:

$$Q = -\frac{2}{\pi}\tan^{-1}\left(\frac{1}{\pi R}\right)$$

$$\lim_{(R \longrightarrow 0)} Q = -1$$

The denominator of equation (D3) becomes unity for a Q of -1 and an R of zero. Therefore, G and G′ become identical for this particular case. The

transfer admittance becomes

$$G'\Big|_{R=0} = \frac{1}{2}\left\{\frac{\sin C - \sin(-C)}{C} - \frac{\sin C + \sin[-(C+\pi)]}{2(C+\pi)} - \frac{\sin C + \sin[-(C-\pi)]}{2(C-\pi)}\right\}$$

$$- \frac{i}{2}\left\{\frac{\cos C - \cos(-C)}{C} - \frac{\cos C + \cos[-(C+\pi)]}{2(C+\pi)} - \frac{\cos C + \cos[-(C-\pi)]}{2(C-\pi)}\right\}$$

$$= \frac{1}{2}\left[\frac{2\sin C}{C} - \frac{2\sin C}{2(C+\pi)} - \frac{2\sin C}{2(C-\pi)}\right]$$

$$G'\Big|_{R=0} = \frac{\pi^2 \sin C}{C(\pi^2 - C^2)} \qquad (2)$$

The limit on G' as R tends to infinity is found as follows:

$$Q = -\frac{2}{\pi}\tan^{-1}\left(\frac{1}{\pi R}\right)$$

$$\lim_{(R\longrightarrow\infty)} Q = 0$$

For a Q of zero and a very large R, the denominator of equation (D3) approaches R. Therefore, for this particular case, equation (D3) is rewritten as

$$\lim_{(R\longrightarrow\infty)} G' = \frac{\lim_{(R\longrightarrow\infty)} G}{R}$$

The limiting process assumes that S becomes very small compared to D, and that C is very small. This results in

$$RC = \frac{n\pi S}{L} \times \frac{D}{S} = \frac{n\pi D}{L}$$

Furthermore, all terms with R (but not the product RC) in the denominator go to zero. The transfer admittance approaches

$$\lim_{(R\longrightarrow\infty)} G' = \frac{1}{1 + iRC} \qquad (3)$$

APPENDIX E

SIMULATION OF THE SCANNING TRANSFER FUNCTION

The theoretical transfer-function method of analyzing the scanning process is a valid, useful, and powerful tool. However, it is sometimes easier to visualize the results by looking at actual wave forms. It is frequently difficult and expensive to change components in a flying-spot scanner to study the effects of different components. There may be nonlinear functions operating in the system. All of these problems can be quickly and easily circumvented by setting up the problem on an analog computer. This procedure allows variables such as phosphor decay, spot size, optical transfer function, and film characteristics to be varied at will for purposes of analysis. Furthermore, signal-processing functions intended to enhance the quality of the video signal can be programed easily, and the results obtained immediately without constructing actual video circuits.

A crude, first-order approximation of the scanning transfer function was programed on a general-purpose analog computer to determine the feasibility of this approach. In addition, the signal-processing technique developed in reference 7 was programed. Delay lines were constructed by using an on-line digital computer with analog-to-digital and digital-to-analog converters. Each input data point was stored in memory and read out a fixed time later; the fixed time was the delay time. Strip-chart records of the simulated video signal were obtained both before and after processing. The output signal was compared with the input signal, and the results were found to be useful.

Figure E-1 shows the essential analog elements needed to simulate a scanning spot having the profile shown in figure E-2. The input signal represents the actual point-by-point transmission of a scanned transparency. Delay line D-1 has a delay time of spot size divided by scan speed. The time constant of integrator I-1 with feedback through P-1 is set equal to the decay time constant of the phosphor. Assume a scanning spot is traveling along an opaque portion of a transparency just on the verge of entering a transparent portion. If the transition is abrupt, the input signal to this circuit will be a step. As the spot itself begins crossing the boundary, integrator I-2

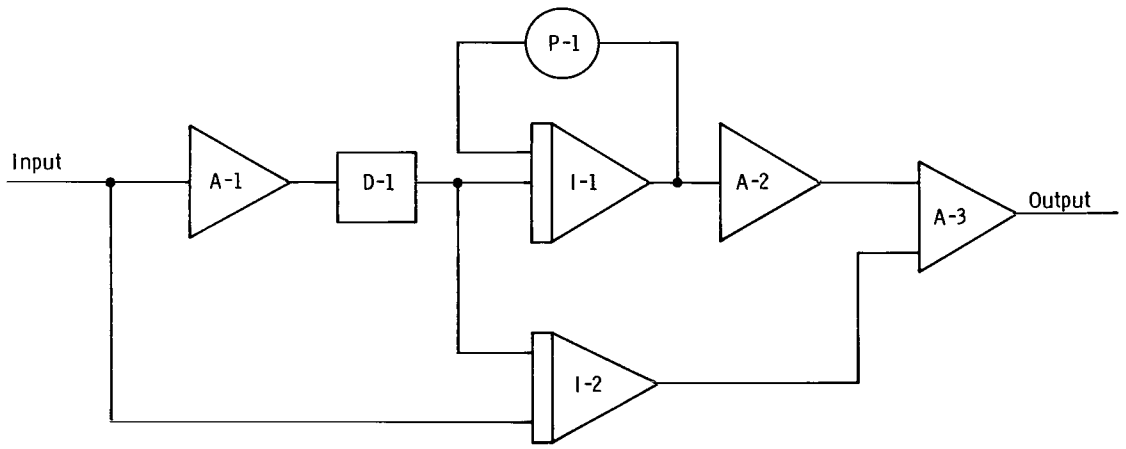

Figure E-1.– Analog computer program simulating a scanning spot.

APPENDIX E

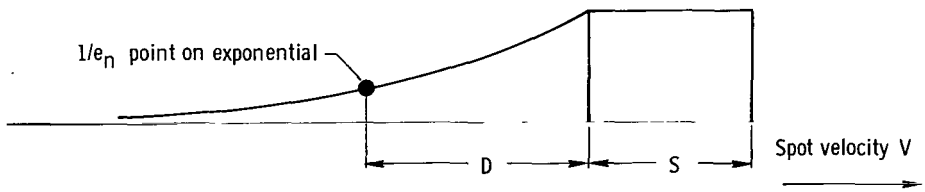

Figure E-2– Profile of uniform scanning spot with decay.

generates a ramp, simulating the constantly increasing amount of transmitted light. When the entire spot has crossed the boundary, the delay line produces the negative of the input signal, thus forcing integrator I-2 to stop integrating and hold its output constant. Simultaneously, integrator I-1 begins an exponential curve initially having the same slope as integrator I-2 had just before it stopped. Integrator I-1 reaches a maximum output after a long enough time, and the difference in the outputs of I-1 and I-2 is the analog of the quantity of transmitted light.

The effects of varying scan velocity and varying spot size are observed by changing the length of the delay line. The input signal frequency is the spatial frequency of the detail on the transparency divided by scan velocity. Thus, to simulate the effects on spatial detail of increased scan velocity, the delay time must be decreased and the input frequency increased proportionately.

Figure E-3 shows the analog circuit devised to simulate the signal-processing technique developed in reference 7. Essentially, the input to this circuit is delayed, multiplied by a constant less than one, and subtracted from the unmodified input. The delay time is chosen arbitrarily, but its choice determines the highest frequencies that will be present in the output. Generally speaking, this delay time is of the same order as the period of the highest output frequencies. The constant multiplier of the delayed signal is $\exp(-t_p/t_d)$ where

t_p delay time of delay line D-2

t_d decay time constant of phosphor determined by the setting of P-1 in figure E-1

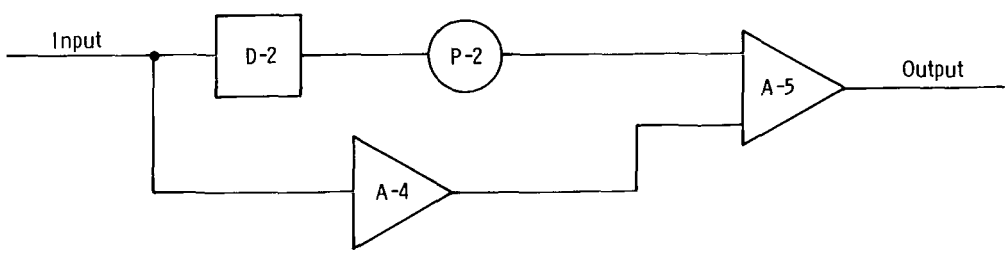

Figure E-3.– Analog computer program simulating a signal-processing technique.

Figures E-4 and E-5 show some strip-chart results obtained from this program. The uppermost trace in each figure is the input signal representing transparency density. The center trace is the result of the scanning process, and the lower trace shows the result of the center trace being passed through the signal-processing circuit.

Generally speaking, figure E-4 shows results when the spot is small compared to the decay tail. The response is roughly that of a simple resistor-capacitor filter. Figure E-5 shows what happens when the spot is large compared to the decay tail. Here the transfer function looks quite different from the simple filter. To further illustrate the distortion due to scanning, a series of random pulses is used as the input. It is also observed that the signal-processing circuit performs well for a relatively small spot but is inadequate for a large spot.

In order to achieve the same output signal level from the signal-processing circuit as the input level, a steady-state gain of 8.5 is required. Higher gain is required at higher frequencies. Thus the signal-to-noise ratio of the output may be unacceptably low. This problem is not obvious in this simulation, but its effects could easily be incorporated by a properly programed noise generator. Other refinements can also be incorporated to provide a more complete program which would be a valuable analysis tool.

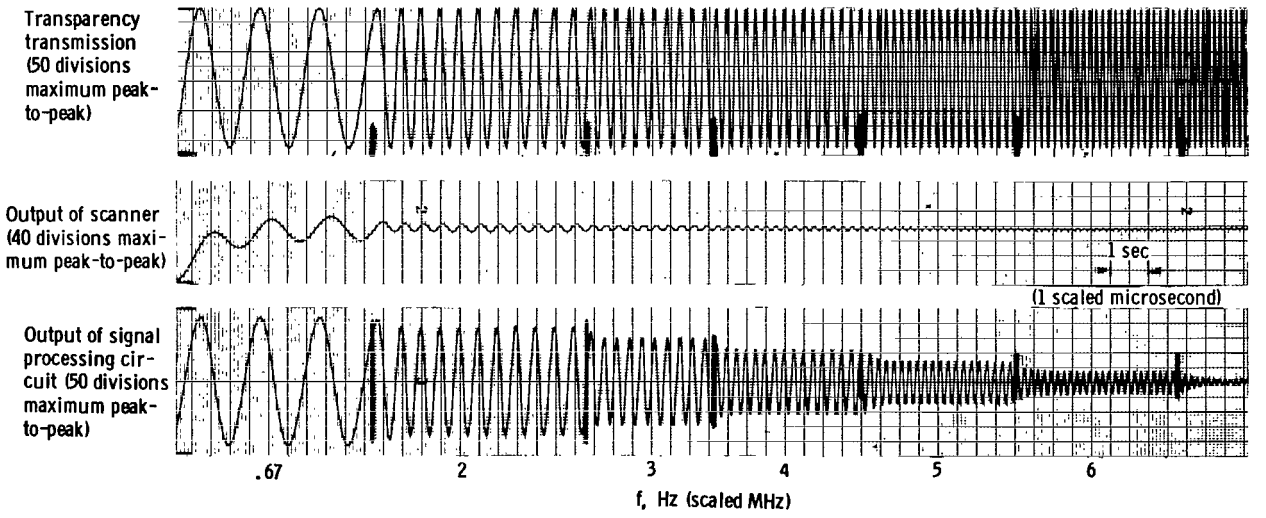

Figure E-4.– Strip-chart record of analog computer simulation of scanning and signal-processing transfer functions for small spot and large decay tail. Motion, right to left; spot size, 0.075 mm; phosphor decay time, 1 microsecond; signal-processing time delay, 0.125 microsecond; scan time, 45 microseconds per scan line; scan line length, 27 mm; actual chart speed, 10 divisions per second; scaled chart speed, 10 divisions per microsecond.

APPENDIX E

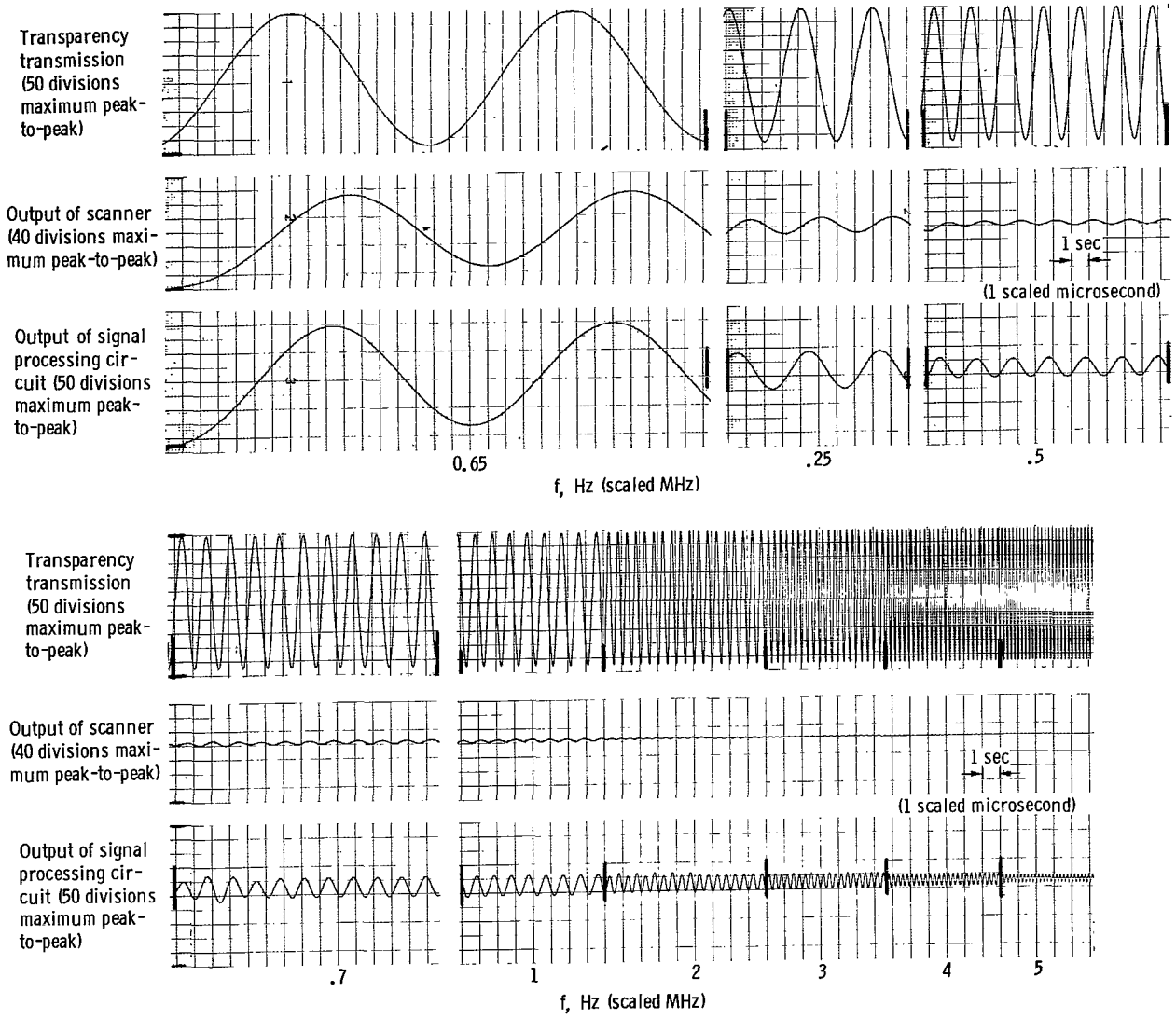

(a) Sine wave input.

Figure E-5.– Strip-chart record of analog computer simulation of scanning and signal-processing transfer functions for large spot and small decay tail with sine wave or random pulse input. Motion, right to left; spot size, 0.075 mm; phosphor decay time, 1 microsecond; signal-processing time decay, 0.125 microsecond; scan time, 45 microseconds per scan line; scan line length, 0.675 mm; actual chart speed, 5 divisions per second; scaled chart speed, 5 divisions per second.

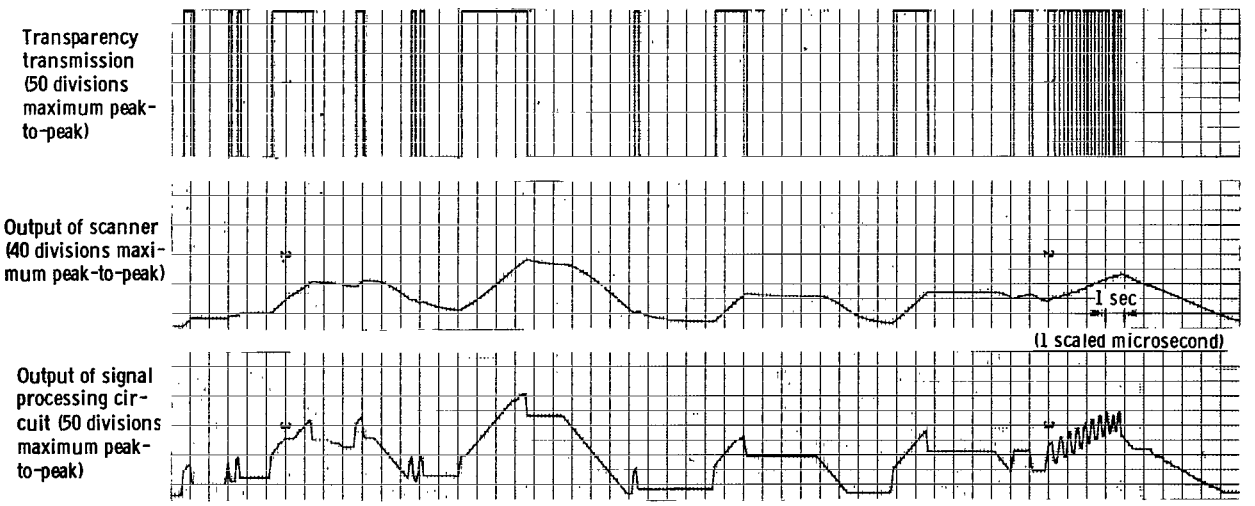

(b) Random pulse input.

Figure E-5.– Concluded.

APPENDIX F

COMPUTATION OF LIGHT-OUTPUT VARIATION WITH SCAN VELOCITY

Assuming that a uniform electron beam is scanning a phosphor screen, light output is a function of rise time, decay time, and scan velocity. Assuming further that both the rise and decay curves are simple, single-component exponentials, the spot-brightness profile B will be that shown in figure F-1 with t_u being the rise-time constant and t_d the decay-time constant.

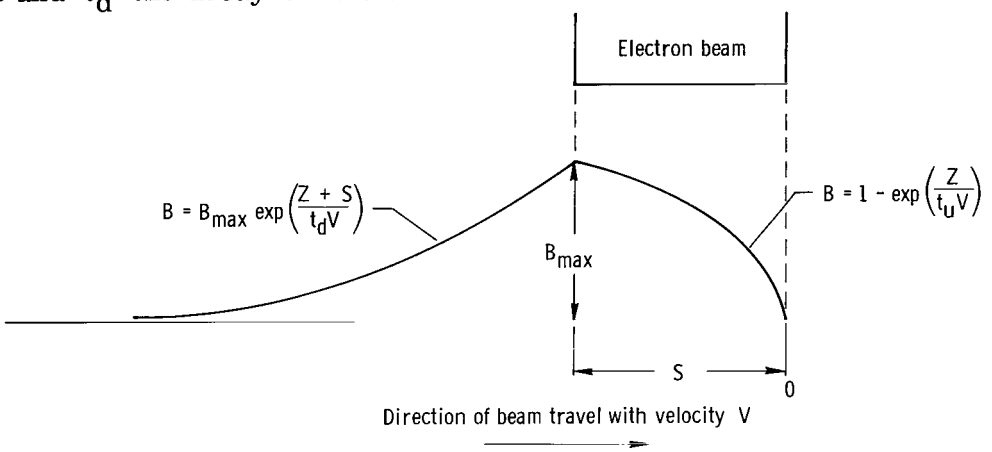

Figure F-1.– Profile of scanning spot showing rise and decay effects.

The total light emitted by the spot is the total integral under both segments of the profile and is expressed as

$$I = \int_{-S}^{0} \left[1 - \exp\left(\frac{Z}{t_u V}\right)\right] dZ + B_{max} \int_{-\infty}^{-S} \exp\left(\frac{Z + S}{t_d V}\right) dZ$$

where

$$B_{max} = 1 - \exp\left(\frac{-S}{t_u V}\right)$$

Integrating yields

$$I = S + V(t_d - t_u)\left[1 - \exp\left(\frac{-S}{t_u V}\right)\right] \qquad \text{(F1)}$$

This expression first shows that if rise time equals decay time, the light output is constant regardless of scan velocity. Taking the limit as V goes to zero, it is seen that the light output has a limit S, depending solely on spot size. This agrees with intuitive reasoning, because rise and decay effects are negligible at slow enough scans. The limit of equation (F1) as V goes to infinity is as follows:

$$\lim_{(V\to\infty)} I = \lim_{(V\to\infty)} \left\{ S + V(t_d - t_u)\left[1 - \exp\left(\frac{-S}{t_u V}\right)\right]\right\}$$

$$= \lim_{(V\to\infty)} \left[S + V(t_d - t_u)\left(1 - 1 + \frac{S}{t_u V} - \frac{S^2}{t_u{}^2 V^2} + \text{terms in } \frac{1}{V^m}\right)\right]$$

$$= \lim_{(V\to\infty)} \left[S + (t_d - t_u)\left(\frac{S}{t_u} - \frac{S^2}{t_u{}^2 V} + \text{terms in } \frac{1}{V^{m-1}}\right)\right]$$

$$= S + \frac{S(t_d - t_u)}{t_u}$$

where m is an integer greater than or equal to 3.

Therefore

$$\lim_{(V\to\infty)} I = S\left(\frac{t_d}{t_u}\right)$$

It is seen that the light output will reach a limit with increasing scan velocity, which will be the light output at minimum velocity multiplied by the ratio of decay time to rise time.

APPENDIX G

CALCULATION OF APERTURE ERROR IN SLIT SCANNING

When scanning a slit with a CRT spot for the purpose of measuring spot size, it is important that the slit be narrow enough that it will not contribute a significant error to the spot profile. Assuming a spot profile has the shape $1 + \cos \frac{\pi Z}{S}$ (see fig. G-1), a slit having a width W samples the spot. The integral under the spot-profile curve between $Z - \frac{W}{2}$ and $Z + \frac{W}{2}$ yields the amplitude of the measured curve at position Z. Introducing Z' as a dummy variable of integration, the measured curve becomes

$$T(Z) = \int_{Z-\frac{W}{2}}^{Z+\frac{W}{2}} \left(1 + \cos \frac{\pi Z'}{S}\right) dZ' = W + \frac{S}{\pi} \left\{\sin \left[\frac{\pi}{S}\left(Z + \frac{W}{2}\right)\right] - \sin \left[\frac{\pi}{S}\left(Z - \frac{W}{2}\right)\right]\right\}$$

The main item of interest is how the width between the half-amplitude points on this curve compares with S, the width of the original profile. The maximum value of $T(Z)$, which is found at $Z = 0$, is

$$T(0) = W + \frac{S}{\pi}\left[\sin\left(\frac{\pi W}{2S}\right) - \sin\left(-\frac{\pi W}{2S}\right)\right]$$

$$T(0) = W + \frac{2S}{\pi} \sin\left(\frac{\pi W}{2S}\right)$$

If S' is the measured width at half amplitude, then $T\left(\frac{S'}{2}\right) = \frac{1}{2} T(0)$. It follows that

$$\frac{W}{2} + \frac{S}{\pi} \sin\left(\frac{\pi W}{2S}\right) = W + \frac{S}{\pi} \left\{\sin\left[\frac{\pi}{S}\left(\frac{S'}{2} + \frac{W}{2}\right)\right] - \sin\left[\frac{\pi}{S}\left(\frac{S'}{2} - \frac{W}{2}\right)\right]\right\}$$

The ratio of measured spot size to actual spot size becomes

$$\frac{S'}{S} = \frac{2}{\pi} \cos^{-1}\left[\frac{\sin\left(\frac{\pi W}{2S}\right) - \frac{\pi W}{2S}}{2 \sin\left(\frac{\pi W}{2S}\right)}\right] \tag{G1}$$

This expression is valid only when $\left|\frac{S'}{2}\right| \leq S - \frac{W}{2}$ in order to avoid getting a contribution from the next cycle in the $1 + \cos \frac{\pi Z}{S}$ representation for the original profile

(dashed curves in fig. G-1). Setting $\frac{S'}{2} = S - \frac{W}{2}$ in equation (G1) results in

$$\pi - \frac{\pi W}{2S} = \cos^{-1}\left[\frac{\sin\left(\frac{\pi W}{2S}\right) - \frac{\pi W}{2S}}{2 \sin\left(\frac{\pi W}{2S}\right)}\right]$$

$$-\cos\frac{\pi W}{2S} = \frac{\sin\left(\frac{\pi W}{2S}\right) - \frac{\pi W}{2S}}{2 \sin\left(\frac{\pi W}{2S}\right)}$$

$$\frac{\pi W}{2S} = \sin\left(\frac{\pi W}{S}\right) + \sin\left(\frac{\pi W}{2S}\right)$$

The above implicit equation has an approximate solution of $\frac{W}{S} = 0.87$. Therefore, equation (G1) correctly yields the slit-width error as long as the slit is less than 87 percent as wide as the spot at half amplitude. This in practice covers all cases of interest. Figure G-2 shows a plot of $\frac{S'}{S}$ versus $\frac{W}{S}$ calculated from equation (G1). This curve will readily show the error introduced by scanning a finite slit with a CRT spot. It is observed that with a slit 80 percent of the spot size, only a 10-percent error is introduced.

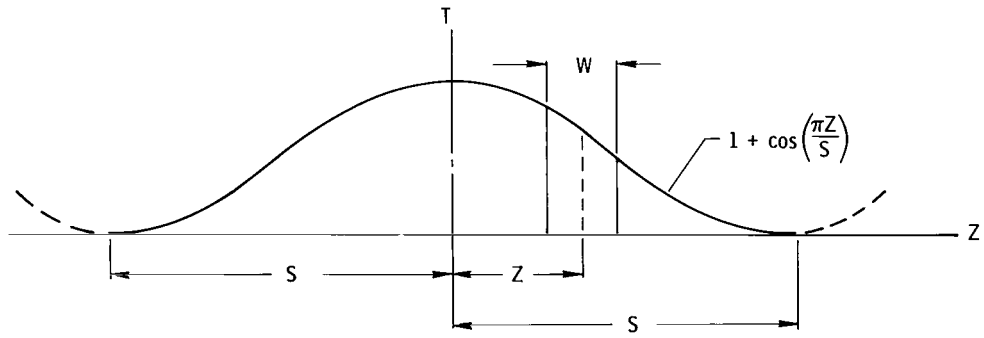

Figure G-1.– Cosine spot profile with sampling aperture.

APPENDIX G

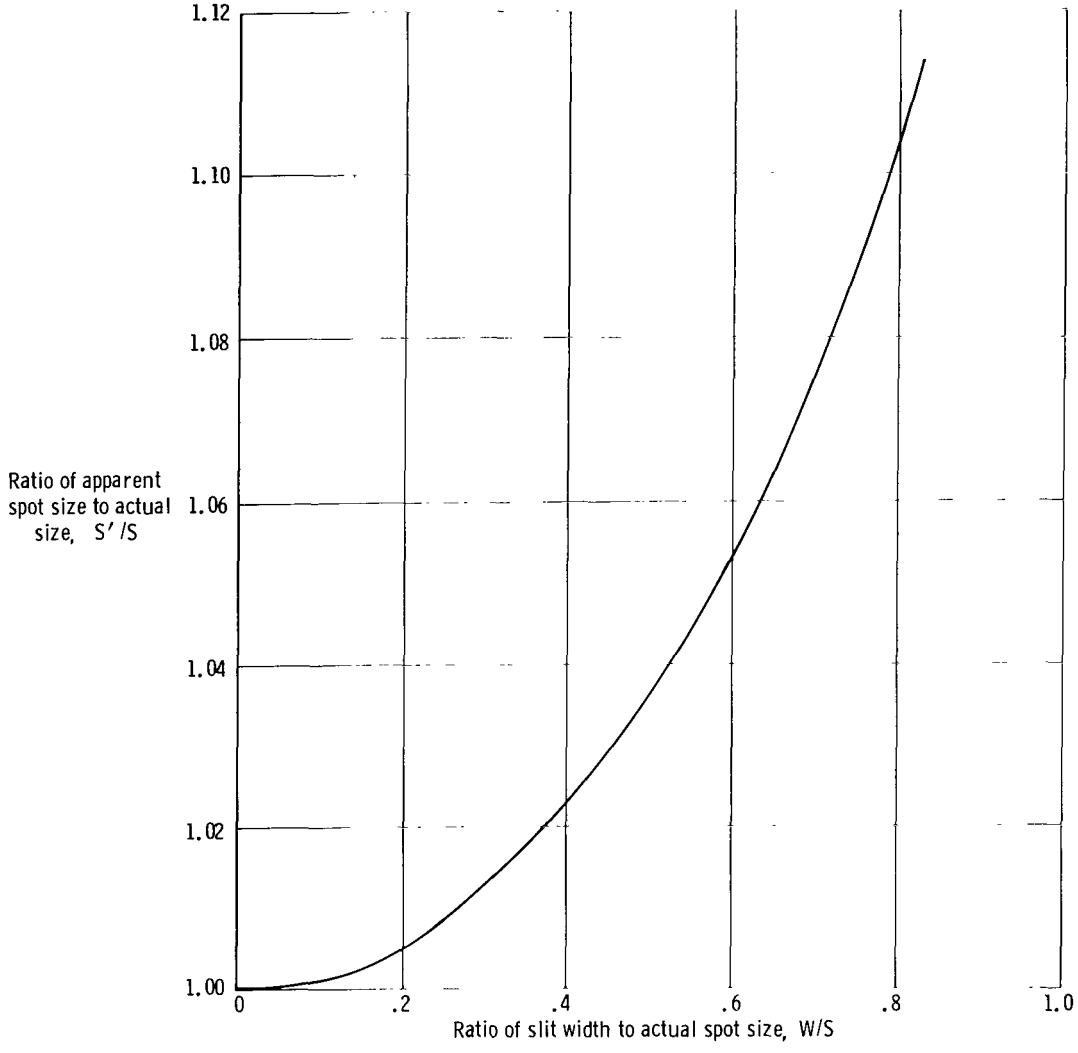

Figure G-2.– Spot-size error due to slit width.

REFERENCES

1. Tucker, A. R.; et al.: Electronic System for Generating a Perspective Image. U.S. Patent Office No. 3,060,596, Oct. 30, 1962.

2. Caligiuri, H. J.: A Study of 3-D Effects in Visual Simulation: Phase I. Tech. Rep. NAVTRADEVCEN IH-53 (DDC No. 635 869), U.S. Naval Training Device Center, June 1966.

3. Mertz, Pierre; and Gray, Frank: A Theory of Scanning and Its Relation to the Characteristics of the Transmitted Signal in Telephotography and Television. Bell System Tech. J., vol. XIII, no. 3, July 1934, pp. 464-515.

4. Dennison, R. C.: Aperture Compensation for Television Cameras. RCA Rev., vol. XIV, no. 4, Dec. 1953, pp. 569-585.

5. Sziklai, G. C.; Ballard, R. C.; and Schroeder, A. C.: An Experimental Simultaneous Color Television System. Part II - Pickup Equipment. Proc. IRE, Sept. 1947, pp. 862-870.

6. Mertz, Pierre: Television—The Scanning Process. Proc. IRE, Oct. 1941, pp. 529-537.

7. Anon.: Experimentation Program for Development of Phosphor for Cathode Ray Tube. Pan Aura Corp. (NASA CR-96002), 1967.

BIBLIOGRAPHY

Anon.: RCA phototubes and photocells. Tech. Manual PT-60, Radio Corp. of America (Lancaster, Pa.), c. 1963.

Brouwer, William: Sine Wave Testing. Optical Spectra, vol. 1, issue 3, Third Quarter, 1967, pp. 71-76.

Brouwer, William: Sine Wave Testing. Part II - Measuring the Transfer Function of a Lens. Optical Spectra, vol. 1, issue 4, Fourth Quarter, 1967, pp. 76-79.

Cawein, Madison: Television Resolution as a Function of Line Structures. Proc. IRE, Dec. 1945, pp. 855-864.

Coltman, J. W.; and Anderson, A. E.: Noise Limitations to Resolving Power in Electronic Imaging. Proc. IRE, vol. 48, no. 5, May 1960, pp. 858-865.

Eberhardt, E. H.: Noise Factor Measurements in Multiplier Phototubes. Applied Optics, vol. 6, no. 2, Feb. 1967, pp. 359-360.

Fink, Donald G.: Television Engineering. Second ed., McGraw-Hill Book Co., Inc., 1952.

Garbuny, Max: Optical Physics. Academic Press, 1965.

Gibson, W. G.; and Schroeder, A. C.: A Vertical Aperture Equalizer for Television. J. SMPTE, vol. 69, no. 6, June 1960, pp. 395-401.

Goldmark, Peter C.; and Hollywood, John M.: A New Technique for Improving the Sharpness of Television Pictures. Proc. IRE, vol. 39, no. 10, Oct. 1951, pp. 1314-1322.

Goodale, E. Dudley; and Kennedy, Ralph C.: Phase and Amplitude Equalizer for Television Use. RCA Rev., March 1949, pp. 35-42.

Herbst, P. J.; Drew, R. O.; and Johnson, S. W.: Electrical and Photographic Compensation in Television Film Reproduction. J. SMPTE, vol. 57, no. 4, Oct. 1951, pp. 289-307.

Jenkins, Francis A.; and White, Harvey E.: Fundamentals of Optics. Third ed., McGraw-Hill Book Co., Inc., 1957.

Kovásznay, L. S. G.; and Joseph, H. M.: Image Processing. Proc. IRE, May 1955, pp. 560-570.

Mansberg, H. P.: Photo-Optical Field Measurement by Flying Spot Scanner for Biomedical Applications. Presented at Eighth Annual Symposium of Society of Photographic Instrumentation Engineers (Los Angeles, Calif.), Aug. 5-9, 1963.

Mertz, Pierre: Perception of Television Random Noise. J. SMPTE, vol. 54, no. 1, Jan. 1950, pp. 8-34.

Pfahnl, Arnold: Properties of Fast-Decay Cathode-Ray Tube Phosphors. Bell System Tech. J., vol. XL11, no. 1, Jan. 1963, pp. 181-201.

Rodda, S.: Photo-Electric Multipliers. MacDonald & Co., Ltd. (London), 1953.

Schade, Otto H.: Electro-Optical Characteristics of Television Systems. RCA Rev.
Part I – March 1948, pp. 5-37.
Part II – June 1948, pp. 245-286.
Part III – Sept. 1948, pp. 490-530.
Part IV – Dec. 1948, pp. 653-686.

Schade, Otto H.: Image Gradation, Graininess and Sharpness in Television and Motion-Picture Systems. J. SMPTE, vol. 64, Nov. 1955, pp. 593-617.

Schroeder, A. C.; and Gibson, W. G.: Television Vertical Aperture Compensation. J. SMPTE, vol. 64, Dec. 1955, pp. 660-670.

Shelton, Carl F.: Spatial Frequency Response of Flying-Spot-Scanner Systems. SPIE J., vol. 5, April-May 1967, pp. 155-160.

Theile, R.; and McGhee, H.: The Application of Negative Feedback to Flying Spot Scanners. J. Brit. Inst. Radio Eng., June 1952, pp. 325-339.

van der Poel, F. H. J.; and Valeton, J. J. P.: The Flying-Spot Scanner. Phillips Tech. Rev., vol. 15, no. 8-9, Feb.-March 1954, pp. 221-232.

Wallace, K. F.; Herbert, J.; and Voss, J.: Final Report - Electrical Readout for Wideband Electron Beam Recording. RADC TDR-62-394, Rome Air Dev. Center, U.S. Air Force, Sept. 27, 1962. (Available from ASTIA as AD 293 201.)

Zimmerman, Jerrold: A Practical Approach Toward The Determination of Resolution Requirements. SPIE J., vol. 4, Aug.-Sept. 1966, pp. 277-280.

Zworykin, V. K., and Morton, G. A.: Television. Second ed., John Wiley & Sons, Inc., c. 1954.

NATIONAL AERONAUTICS AND SPACE ADMINISTRATION
WASHINGTON, D. C. 20546

OFFICIAL BUSINESS

FIRST CLASS MAIL

POSTAGE AND FEES PAID
NATIONAL AERONAUTICS AND
SPACE ADMINISTRATION

"The aeronautical and space activities of the United States shall be conducted so as to contribute . . . to the expansion of human knowledge of phenomena in the atmosphere and space. The Administration shall provide for the widest practicable and appropriate dissemination of information concerning its activities and the results thereof."

—NATIONAL AERONAUTICS AND SPACE ACT OF 1958

NASA SCIENTIFIC AND TECHNICAL PUBLICATIONS

TECHNICAL REPORTS: Scientific and technical information considered important, complete, and a lasting contribution to existing knowledge.

TECHNICAL NOTES: Information less broad in scope but nevertheless of importance as a contribution to existing knowledge.

TECHNICAL MEMORANDUMS: Information receiving limited distribution because of preliminary data, security classification, or other reasons.

CONTRACTOR REPORTS: Scientific and technical information generated under a NASA contract or grant and considered an important contribution to existing knowledge.

TECHNICAL TRANSLATIONS: Information published in a foreign language considered to merit NASA distribution in English.

SPECIAL PUBLICATIONS: Information derived from or of value to NASA activities. Publications include conference proceedings, monographs, data compilations, handbooks, sourcebooks, and special bibliographies.

TECHNOLOGY UTILIZATION PUBLICATIONS: Information on technology used by NASA that may be of particular interest in commercial and other non-aerospace applications. Publications include Tech Briefs, Technology Utilization Reports and Notes, and Technology Surveys.

Details on the availability of these publications may be obtained from:

SCIENTIFIC AND TECHNICAL INFORMATION DIVISION

NATIONAL AERONAUTICS AND SPACE ADMINISTRATION

Washington, D.C. 20546